HOMOGENEOUS AND HETEROGENEOUS REACTIONS IN PLASMAS OF MODERATE PRESSURE

E. MOLINARI

Centro di Studio per la Chimica dei Plasmi del CNR, Istituto di Chimica Generale ed Inorganica dell'Università, Bari, Italy

ABSTRACT

Plasmas in the pressure range 5–50 torr at power densities of 1–10 cal cm^{-3} sec^{-1} are typical of conditions intermediate between those of 'thermal' plasmas and those of 'cold' plasmas. Remarkable disequilibrium exists between electronic, vibrational, rotational and kinetic temperatures, the latter being in the range 700–2000 K. Excited vibrational and rotational levels are populated well above equilibrium and this is regarded as the cause of the high rates observed for the dissociation of molecular species. This point of view allows a rationalization to be made of the kinetic data collected for various reactions both homogeneous (production of H atoms, conversion of methane into acetylene, synthesis of hydrogen cyanide from nitrogen and methane) and heterogeneous (reduction of metal oxides in a hydrogen plasma).

Models for reactions under plasma conditions are presently available for two limiting states of the plasma.

'Thermal' plasmas at pressures around atmospheric are undoubtedly the most extensively studied[1, 2, 3] and satisfactory models for 'cold' plasma reactors at pressures below a few torr have recently been developed and applied to the dissociation of diatomic molecules[4a, b]. It appeared therefore of interest to investigate chemical reactions at pressures in the range 5–50 torr with the aims of bridging the gap between the two limiting conditions of 'thermal' and 'cold' plasmas and of ascertaining whether characteristics peculiar to this intermediate state of the plasma could be utilized efficiently for chemical purposes.

The model developed by Bell[4] for dissociation of diatomic molecules in a 'cold' plasma reactor is based on the assumption that the largest contribution to the process comes from dissociation by direct electron impact $A_2 + e = 2A + e$. In this treatment the rate of atom production is expressed as

$$d[A]/dt = 2\,k^{e}_{A_2} n_e [A_2] = k^{D}_{A_2} [A_2] \tag{1}$$

where $k^{e}_{A_2}$ is given by

$$k^{e}_{A_2} = \left(\frac{8}{\pi m_e}\right)^{\frac{1}{2}} (kT_e)^{-3/2} \int_0^{\infty} \varepsilon \sigma_D(\varepsilon)\, e^{-\varepsilon/kT_e}\, d\varepsilon \tag{2}$$

with n_e denoting electron concentration, m_e electron mass, T_e electron temperature, and ε electron energy. $\sigma_D(\varepsilon)$ is the cross section for A_2 dissociation by direct electron impact. In the derivation of equation (2) a Boltzmann distribution of electron energies has been assumed. The electron temperature T_e is a unique function of the reduced field X/P (volt cm^{-1} $torr^{-1}$) for a given plasma and values of $k^e_{A_2}$ as a function of T_e or X/P calculated by Bell for hydrogen (H_2) are given in *Figure 1*.

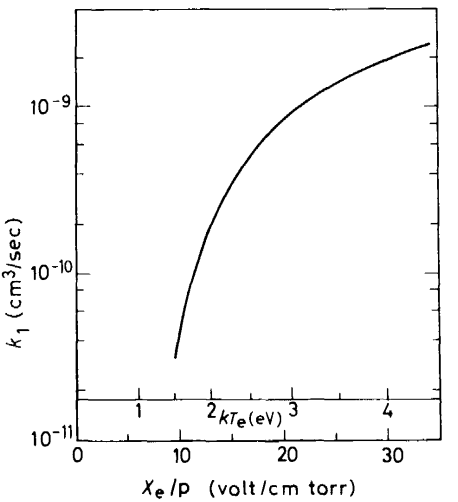

Figure 1. Rate constant for hydrogen dissociation by electron impact as a function of electron temperature and reduced field (Ref. 4a).

Rate constants utilized in 'thermal' plasmas are, in general, values for 'thermal' reactions extrapolated at plasma temperatures. The theoretical calculation of dissociation rates of diatomic molecules represents a complex problem[5–7] and *Figure 2* shows Arrhenius plots of dissociation rates of oxygen (O_2), both measured and calculated[6], in a temperature interval of interest for thermal plasmas. In these plasmas it is possible, in favourable cases, to relate the observed extent of reaction to thermodynamic equilibria prevailing at plasma temperatures and *Figure 3*, taken from ref. 8, is an example of such a correlation.

It should be appreciated that rates of dissociation in 'cold' plasma are plotted against the *electron* temperature T_e in *Figure 1* while these rates have the *gas* temperature T_g as abscissa in 'thermal' plasmas (*Figure 2*). When the pressure is increased at a constant value of the electric field X the reduced field X/P decreases and *Figure 4*, taken from ref. 9, illustrates quite nicely how the total energy provided by the electric field to the plasma is distributed among different elementary processes in oxygen.

This behaviour is essentially a consequence of the dependence of the various cross sections on electron energy and *Figure 5* illustrates this dependence for different cross sections in hydrogen[10].

Plasma conditions utilized in the kinetic studies to be described below

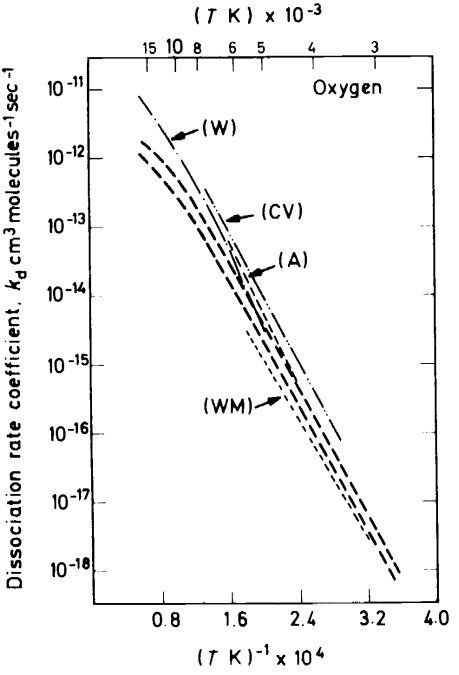

Figure 2. Theoretical and experimental rate constants for oxygen dissociation as a function of gas temperature (Ref. 6).

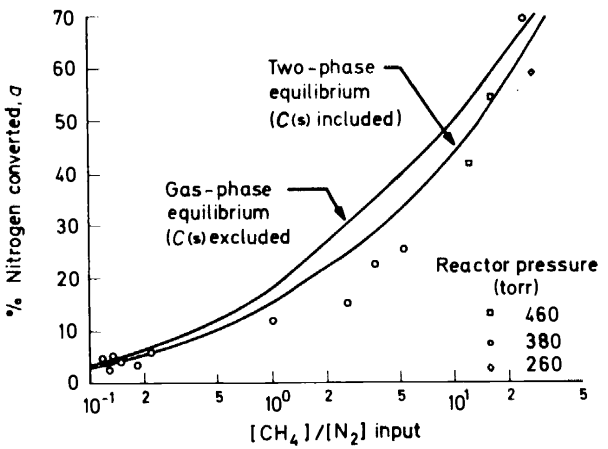

Figure 3. Yield of HCN, expressed as percentage of nitrogen converted, as a function of input stoichiometry (Ref. 8).

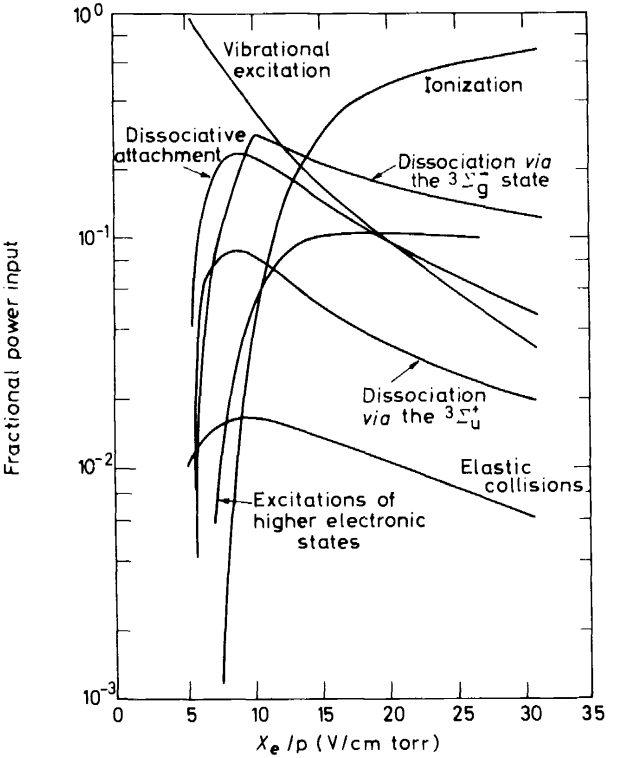

Figure 4. Fractional power input to elastic and inelastic collisions in oxygen as a function of the reduced field (Ref. 9).

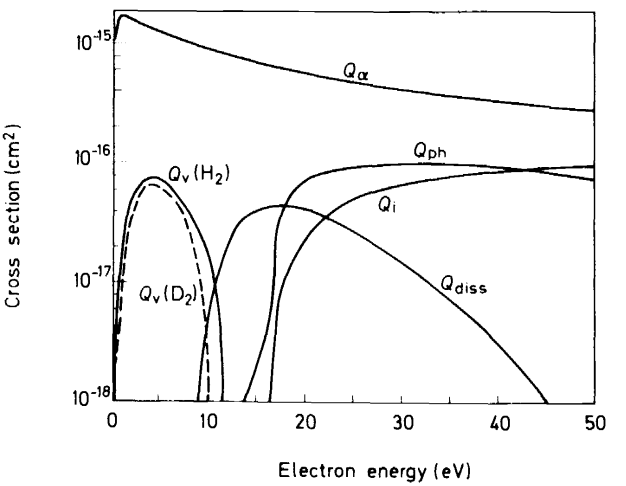

Figure 5. Cross sections for elastic and inelastic collisions in hydrogen and deuterium as a function of electron energy. Q_α, momentum transfer, Q_i, ionization, Q_{diss}, dissociation, Q_{ph}, photon excitation, Q_V, vibrational excitation (Ref. 10).

correspond to electron temperatures at which rotational and vibrational excitation is favoured with respect to other processes. *Figure 6* summarizes the results of a vibro-rotational analysis of the emission of the second positive system of nitrogen $N_2(C^3\Pi_u \rightarrow B^3\Pi_g)$ and of the first negative system of N_2^+ $(B^2\Sigma_u^+ \rightarrow X^2\Sigma_g^+)$ carried on in pure flowing nitrogen at pressures between 5 and 50 torr and at power levels of 1–5 kW[11]. It is quite clear from this

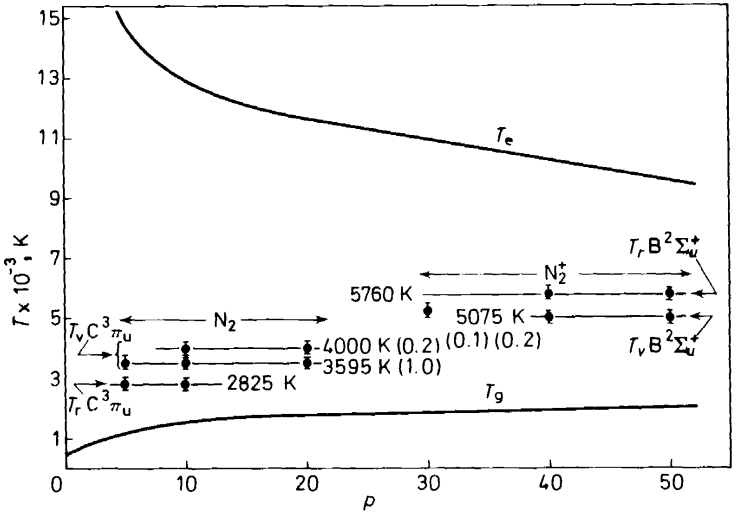

Figure 6. Evaluated electron temperature (T_e) and gas temperature (T_g) and measured rotational (T_r) and vibrational (T_v) temperatures for the $C^3\Pi_u$ state of nitrogen and the $B^2\Sigma_u^+$ state of N_2^+ as a function of pressure (Ref. 11).

figure that strong disequilibrium exists between T_e, T_v, T_r and T_g, with T_g well above room temperature. The plasma cannot therefore be considered 'cold' but the system is a typical non-equilibrium plasma. The distributions of rotational and vibrational energies have been found to be strictly Boltzmann.

When hydrogen is added to the nitrogen stream the first negative system of N_2^+ is suppressed and T_v of the $C^3\Pi_u$ state is lowered by approximately 1 000 K.

The question may now be asked: What would be the consequence of concentrating a part of the available energy in a particular degree of freedom, such as vibration, on the rate of an endothermic reaction? The answer for the reaction $HF + H = H_2 + F$ ($\Delta H = +35$ kcal/mole) comes from *Figure 7*, taken from the work of Polanyi[12]. In this diagram ordinates represent vibrational energies, abscissae rotational energies and diagonals points of equal translational energy. Values of the rate constants are given by contour lines and it can be appreciated that a concentration of the available energy into vibration can increase the rate constant by more than three orders of magnitude. In this connection, it should be remembered that some years ago Burton and Funabashi[13] drew attention to the important role that excitation of internal degrees of freedom might play in the elucidation of the mechanisms of reactions in electrical discharges.

These ideas will be utilized in an attempt to rationalize the kinetic results obtained for the synthesis of HCN from N_2 and CH_4[14], for the conversion of methane into acetylene[15], for the production of hydrogen atoms[16] and for the heterogeneous reduction of metal oxides in a hydrogen plasma[17].

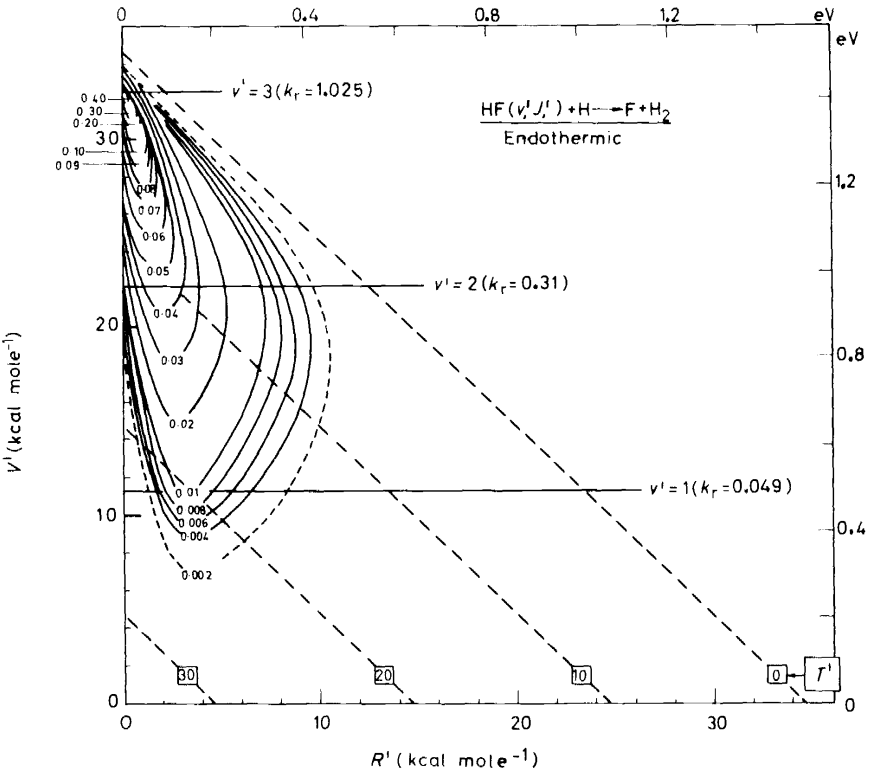

Figure 7. Contours of the rate constants for the endothermic reaction specified, in a plot of vibrational energy V', rotational energy R', and translational energy T' (Ref. 12).

The arrangement of the discharge reactor utilized for the homogeneous reactions is shown in *Figure 8*. The reactor is capacitively coupled to a 35 MHz generator (maximum output 5 kW r.f.) by means of external sleeve electrodes of copper which can be positioned at different separations L. The inner tube of either quartz or Pyrex is surrounded by a water jacket which is also used for calorimetric purposes. In most of the experiments the inner diameter of the tube was 4 cm but tubes of 7.5 cm have also been utilized. Gas sampling was performed by means of thin tubes of alumina positioned at different distances l from the upper edge of the upper electrode and against the reactor's wall.

Sampling within the discharge was also possible by means of a water cooled probe of special design. The reacted gases collected from the various probes were quantitatively analysed gas-chromatographically.

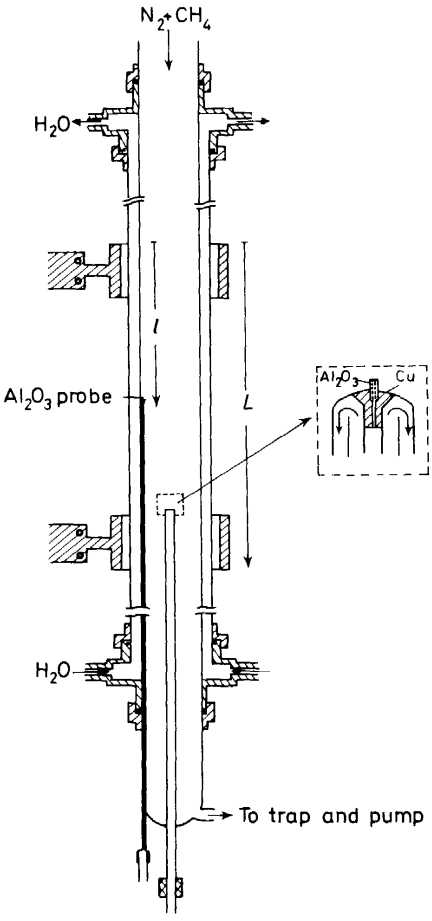

Figure 8. The discharge reactor (Ref. 14a).

THE SYNTHESIS OF HCN

The data of *Figure 9* show the results of thermodynamic calculations of the percentage conversion into HCN as a function of temperature for conditions of pressure and composition included in the experiments. The fact that *kinetic* rather than *thermodynamic* considerations should be utilized in order to interpret the experimental results emerges quite clearly from the following observations. In *Figure 10(a)* the percentage conversion of CH_4 into HCN, β, has been plotted as a function of W_s. W_s is the power collected by the water jacket W_{H_2O} (kcal/sec) divided by the mass flow (g/sec) and the different curves refer to different sampling positions along the reactor's axis (1–4) and to different electrode separations L (full and broken curves).

From the data of *Figure 10(a)*, the data of *Figures 10(b)* and *10(c)* are easily calculated. This figure is typical of the observations made for all conditions and shows that concentration profiles develop along the reactor's axis

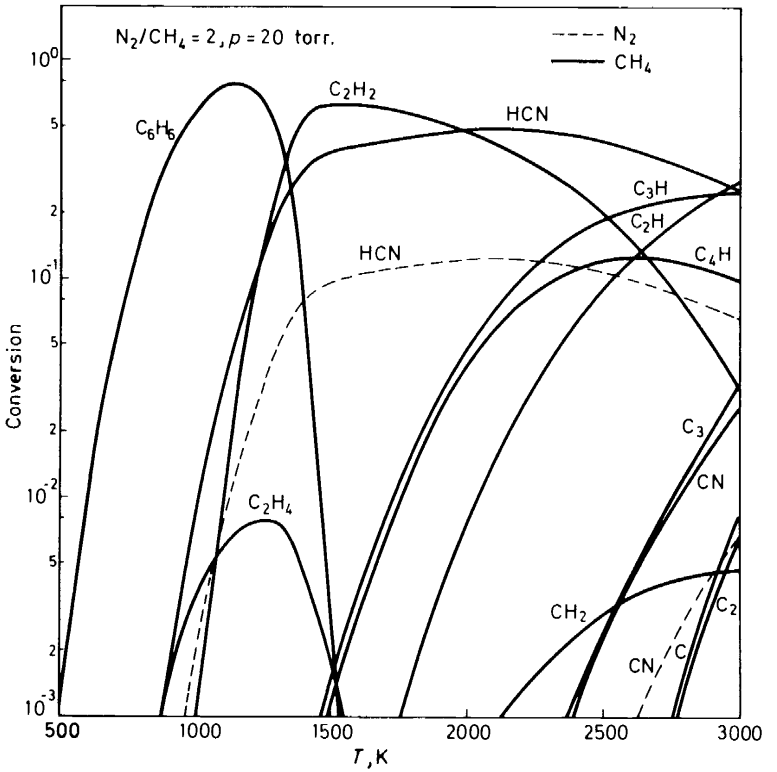

Figure 9. Percentage conversion of methane (full lines) and of nitrogen (broken lines) into various species calculated from equilibrium compositions at different temperatures. ($[N_2]/[CH_4] = 2$, 20 torr) (Ref. 14a).

which are determined by the specific power input W_s. The fact that W_s rather than W_{H_2O} should be considered a parameter for the reaction under discharge conditions is unambiguously shown by the data of *Figure 11*. Values of β determined from sampling at the lower end of the reactor (Probe C) and at $l/L = \frac{1}{2}$ (Probe 2) are collected in *Figure 12*, while *Figure 13* shows the influence of the initial composition. The marks on the ordinate scale give the maximum βs calculated from thermodynamics. In the range of pressures investigated these results therefore show that a concentration profile develops along the reactor's axis and that values of β determined at the reactor's end can *exceed* thermodynamic values and approach complete conversion ($\beta = 1$).

Energy yields for this reaction are collected in *Figure 14* which again shows the detrimental influence of CH_4 (compare with *Figure 13*).

An observation which is of fundamental importance for the elucidation of the mechanism is that the conversion of CH_4 into C_2H_2 was found to occur within a very short distance along the reactor's axis at the small flow-rates utilized in the experiments [less than 500 cm^3 (s.t.p.)/min]. It is therefore apparent that the reaction leading to HCN involves C_2H_2 rather than CH_4.

From a thermodynamic point of view the more endothermic step of the reaction is: $CH_4 \rightarrow \frac{1}{2} C_2H_2 + 1.5\, H_2$ with $\Delta H = +45$ kcal/mole while the reaction $\frac{1}{2} C_2H_2 + \frac{1}{2} N_2 \rightarrow HCN$ requires 4 kcal/mole. The conversion of methane into acetylene must therefore be strongly favoured kinetically, while the subsequent reaction with N_2 is kinetically hindered and is likely to involve the dissociation of N_2 which might then represent a comparatively slow controlling step.

From the above considerations one can draw the following conclusions: (1) It is necessary to establish a rate expression for the synthesis under discharge conditions and to interpret the behaviour of rate constants as a

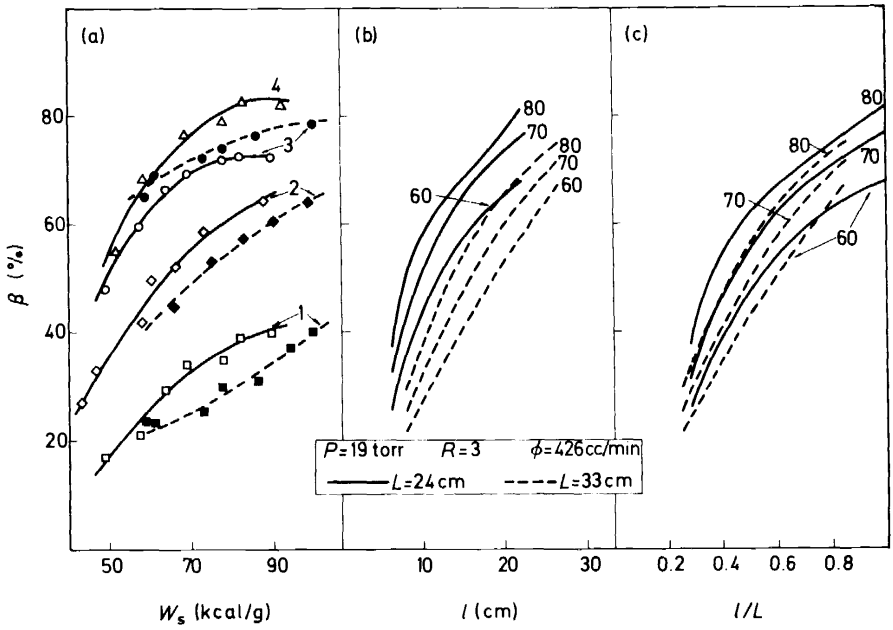

Figure 10. (a) Percentage conversion of methane into hydrogen cyanide β versus W_s as determined by sampling from probes 1, 2, 3, 4 placed at increasing axial distance l. Values of L as specified. (b) β versus l for the specified values of L and the values of W_s marked on the curves. (c) β versus reduced length l/L. (Ref. 14a).

function of the various discharge parameters. This will be done in the following pages. (2) It is necessary to establish how non-equilibrium conditions in these plasmas (e.g. illustrated by *Figure 6*) modify pseudo-equilibrium or steady-state concentrations of the various species with respect to their values at thermodynamic equilibrium at the kinetic gas temperature T_g. This will not be done here, but reference can be made to the general problem as recently treated by Vepřek[18].

The overall rate of the reaction of nitrogen atoms with acetylene can be written as: $d[HCN]/dt = k[N][C_2H_2]$ and it can be shown[14b] that under discharge conditions and for $[N] \ll [C_2H_2]$ the steady-state expression for

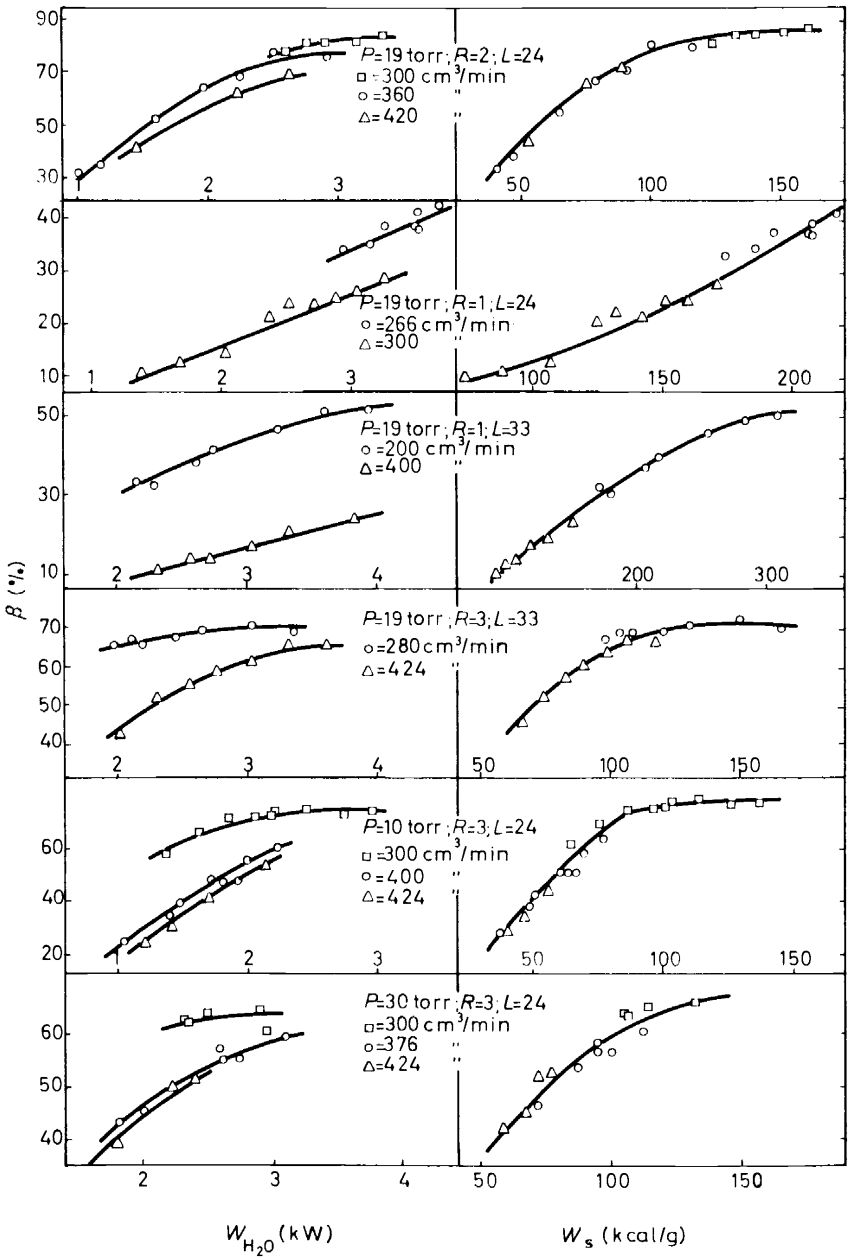

Figure 11. Percentage conversion (β) as a function of power (W_{H_2O}) (left) and of W_s (W_{H_2O}/mass flow) (right) for various gas flowrates at different pressures, compositions and electrode separations (Ref. 14a).

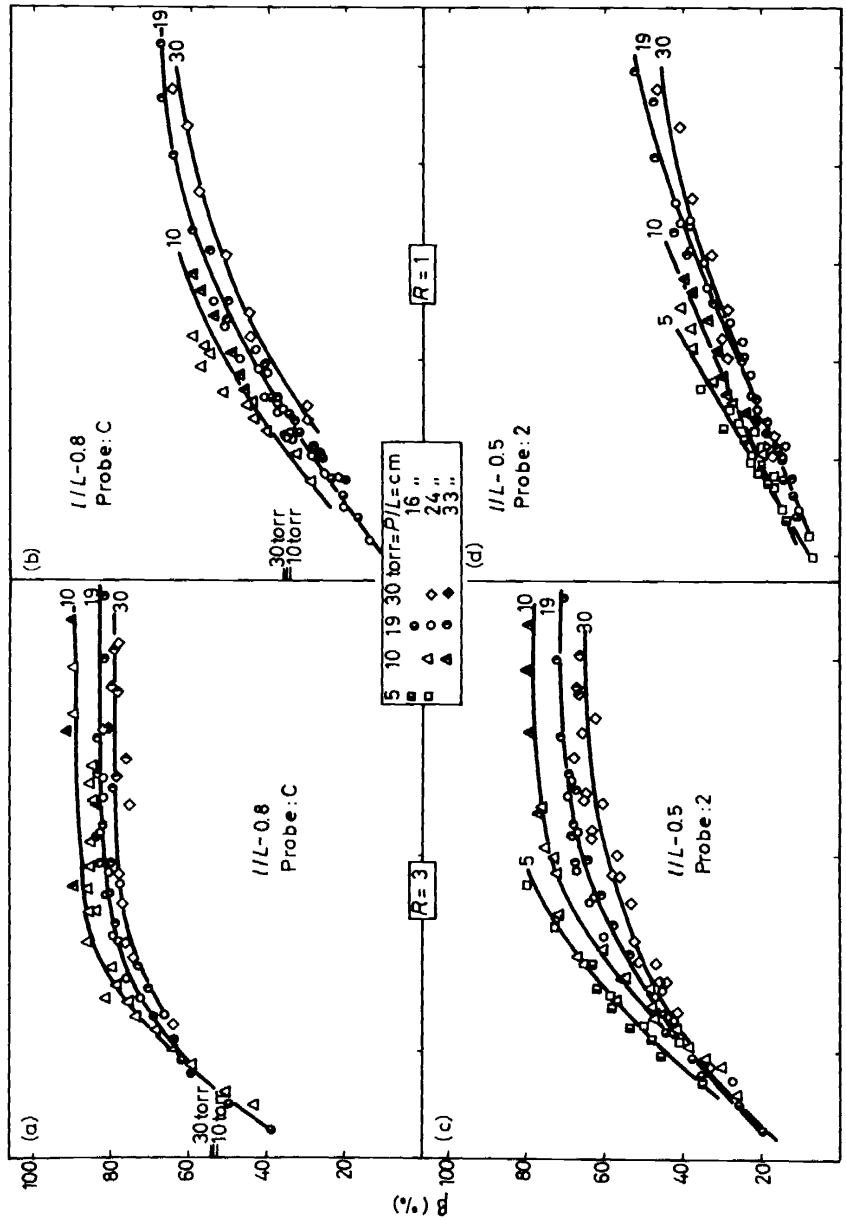

Figure 12. Percentage conversion (β) as a function of W_s for pressures marked on the curves. Marks on the ordinates give maximum thermodynamic values (Ref. 14a).

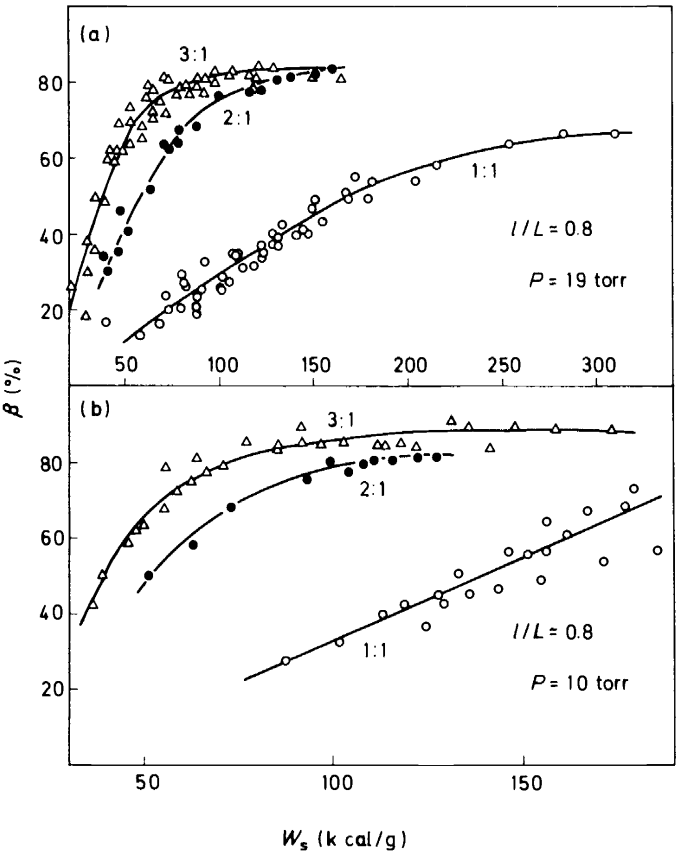

Figure 13. Percentage conversion (β) versus W_s for various $[N_2]/[CH_4]$ ratios at 19 and 10 torr (Ref. 14a).

the reaction rate is given, in terms of the percentage conversion β, by the kinetic equation

$$d[HCN]/dt = k^{D}_{N_2}\{[N_2]^\circ - \beta[C_2H_2]^\circ\} \tag{3}$$

where $k^{D}_{N_2}$ is the first order rate constant for the production of N atoms within the discharge. Integration of equation (3) requires a knowledge of the distribution of residence times within the reactor. For an isothermal *plug flow* reactor integration gives

$$\ln\{2R/(2R - \beta)\} = \tfrac{1}{2}k^{D}_{N_2}\theta \tag{4}$$

where $2R = 2[N_2]^\circ/[CH_4]^\circ = [N_2]^\circ/[C_2H_2]^\circ$ and $\theta = \pi r_T^2 l/\phi$ (sec) with r_T the tube radius, l the axial distance, ϕ the volumetric flowrate ($cm^3\ sec^{-1}$, at pressure P and gas temperature T_g). The rate expression for a *stirred tank* reactor can be written

$$\beta/(2R - \beta) = \tfrac{1}{2}k^{D}_{N_2}\pi r_T^2 L/\phi \tag{5}$$

with L the electrode spacing. Equation (5) can be made parametric in l in order to express the dependence of β on the axial distance l. In this case the equation loses its physical meaning but can be utilized as a suitable approximation to a more complex integrated equation in which the actual distribution of residence times is explicitly considered. In particular, a residence time distribution corresponding to a *laminar flow* reactor can, in favourable cases, yield an integrated rate expression which can be approximated by means of equation (5) in parametric form.

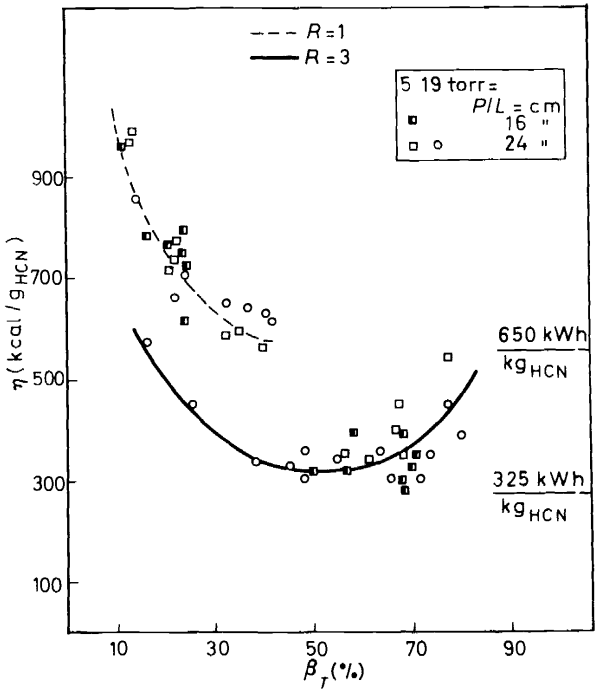

Figure 14. Energy yield η for the production of hydrogen cyanide versus percentage conversion (Ref. 14a).

Values of β determined as a function of l have been plotted in *Figure 15* according to either equation (4) or (5) for various conditions and for a $[N_2]/[CH_4]$ ratio $R = 1$. At 19 torr equation (5) is followed quite closely while at 5 torr the plug flow equation (4) should be used to fit the data.

The slope of these straight lines is $\frac{1}{2}k^{D}_{N_2}\pi r_T^2/\phi$, from which values of $k^{D}_{N_2}$ can be derived once the gas temperature T_g is known ($\phi = \phi(P, T_g)$). Under the above conditions one is therefore measuring the *rate of dissociation of nitrogen* within the discharge which is now seen to represent the slowest step of the reaction.

The situation for a 3/1 mixture is somewhat more complex, as discussed in ref. 14b, but still allows us to derive values of $k^{D}_{N_2}$. A model for this reaction under plasma conditions should allow prediction of values of $k^{D}_{N_2}$ and their dependence on discharge parameters and gas temperature T_g.

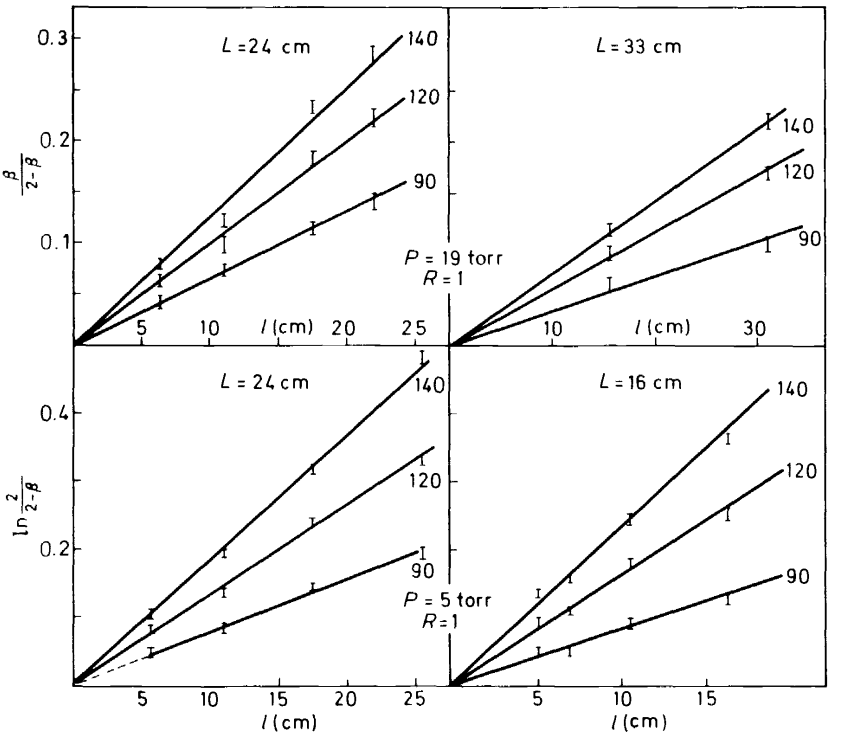

Figure 15. Plots of percentage conversion (β) as a function of the axial distance according to equations [4] (5 torr) and [5] (19 torr) for $[N_2]/[CH_4] = 1$ at different W_s (kcal/g) (Ref. 14b).

THE MODEL DISCHARGE

The discharge has been assumed to be isothermal and axially and radially uniform. This is a rather severe approximation, the consequences of which will be explained below. A detailed treatment of the problem is given in ref. 14b and only the main features of the model will be examined here.

In view of the rapid conversion of methane into acetylene initial conditions are those of a plasma of H_2, N_2 and C_2H_2. The approximation is made that the power delivered to the plasma by the electric field is mainly utilized for the dissociation of H_2 molecules and that the power collected by the water jacket between the electrodes is essentially made up of two contributions: the heterogeneous recombination of hydrogen atoms at the walls and thermal conduction from the isothermal plasma. This approximation has been found to be valid for most of the conditions examined. The following balance equations can then be written:

$$W_{H_2O} = q_H + q_\lambda \tag{6}$$

with

$$q_H = [k_H \delta_H/(k_H + \delta_H)][H] \times 52 \times 10^3 \times 2\pi r_T L$$

where the term $k_H\delta_H/(k_H + \delta_H)$ represents the rate constant for a first order heterogeneous recombination on the walls of the hydrogen atoms at concentration [H] in the presence of diffusion limitations. q_λ is: $q_\lambda = h(T_g - T_w) \times 2\pi r_T L$ with h the coefficient of heat transfer for cylindrical geometry and T_w the wall temperature.

$$\langle W_{H_2O} \rangle = k^D_{H_2}[H_2] \times 52 \times 10^3 \tag{7}$$

where $\langle W_{H_2O} \rangle$ is the power density (cal cm^{-3} sec^{-1}) in the plasma, $k^D_{H_2}$ the first order rate constant for the dissociation of molecular hydrogen within the discharge, $[H_2]$ is the concentration of H_2 and 52×10^3 is half the dissociation energy of H_2, as in equation (6). The steady-state concentration of hydrogen atoms within the discharge obeys the following equation:

$$k^D_{H_2}[H_2] = k'[H] + k''(N_T - [H])\,[H]^2 + k'''\,[H]^3 \tag{8}$$

where the term $k'[H]$ accounts for atom losses due to wall recombination and the other terms represent atom losses due to trimolecular and triatomic homogeneous recombinations. For $[N] \ll [C_2H_2]$ the mass balance is:

$$\begin{gathered}[N_2] + [H_2] + [H] + [C_2H_2] + [HCN] = N_T \\ \frac{[N_2] + \frac{1}{2}[HCN]}{2[C_2H_2] + [HCN]} = \frac{[N_2]^\circ}{[CH_4]^\circ} = R; \quad \frac{[N_2] + \frac{1}{2}[HCN]}{[H_2] + \frac{1}{2}[H]} = \frac{R}{1.5} \\ \frac{[HCN]}{2[C_2H_2] + [HCN]} = \beta\end{gathered} \tag{9}$$

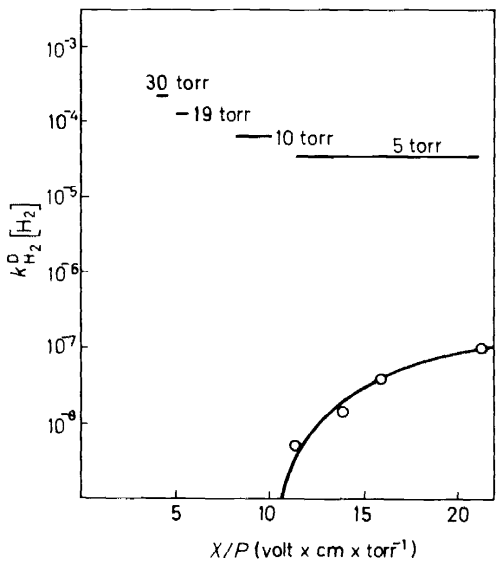

Figure 16. Rates of hydrogen dissociation as a function of the reduced field as derived from experiments at different pressures and calculated according to Ref. 4 at 5 torr (circles) (Ref. 14b).

From equations (6) to (9) the four unknowns $[H_2]$, $[H]$, T_g and $k^D_{H_2}$ can be calculated by a trial and error procedure, all constants being rather complex functions of T_g. Once a value of T_g has been calculated corresponding values of $k^D_{N_2}$ can be derived from plots of the type shown in *Figure 15*.

Values of $k^D_{H_2}$ and $k^D_{N_2}$ derived from the experiments as specified above can now be compared with the corresponding values calculated for either 'thermal' or 'cold' plasmas.

It has been shown[14b] that a purely thermal mechanism is unable to account for the observed rates of production of hydrogen and nitrogen atoms in the discharge, in that it would require temperatures incompatible with the known properties of these plasmas and should be completely ruled out.

The mechanism discussed by Bell for cold plasmas[4] is also unable to account for the observed rates of hydrogen dissociation. This can be appreciated from *Figure 16* where rate constants $k^D_{H_2}$ have been plotted as a function of the reduced field strength X/P and compared with values calculated according to Bell at 5 torr.

This mechanism is unable to account for the measured rates in that values of X/P, hence of T_e, are too small in the pressure range investigated for dissociation by direct electron impact to make a significant contribution to molecular dissociation.

The above results give a clear indication that under the conditions of moderate pressure of the present discharges a mechanism of molecular dissociation characteristic of the 'intermediate' state of the plasma should be operating, different from either purely thermal or purely electron impact dissociation.

In order to derive an expression for $k^D_{H_2}$ and $k^D_{N_2}$ valid for the range of moderate pressure investigated a mechanism of molecular dissociation has been proposed[14b] and will be illustrated below.

In order to simplify the problem we shall make the approximation of a quasi-continuum of vibro-rotational levels of equal weight between the zero energy level and the dissociation limit of the molecule and write a Boltzmann distribution of the molecules among these levels characterized by a unique vibro-rotational temperature T_ξ

$$\frac{dC_{ij}(\xi)}{C_{ij}} = \exp(-\xi/RT_\xi)\frac{d\xi}{RT_\xi} \tag{10}$$

where ξ is the energy of the level. It will furthermore be assumed that T_ξ is the same for all molecular species present in their ground electronic state.

We shall now consider that dissociation may take place from any vibro-rotationally excited level. The rate of atom production from the set of excited molecules ij^* with energies between ξ and $\xi + d\xi$ will be given by

$$dV_{ij}(\xi) = 2k_{ij}(\xi) \times N_T \times dC_{ij}(\xi) \tag{11}$$

If we make use of the naïve idea that the relative kinetic energy between the molecule and the third body must supply the *energy difference* between the dissociation energy E_{ij} and the energy of the vibro-rotational level ξ one can write

$$k_{ij}(\xi) = k^\circ_{ij} \exp[-(E_{ij} - \xi)/RT_g] \tag{12}$$

The overall rate of atom production from ij is obtained by integration of (11) after substitution from (10), (12) and for T_ξ sufficiently higher than T_g:

$$V_{ij} = k_{ij}^{D} C_{ij} = 2k_{ij}^{\circ} \times N_T \times C_{ij} \int_0^{E_{ij}} \exp\left[-(E_{ij} - \xi)/RT_g\right] \times \exp(-\xi/RT_\xi) \frac{d\xi}{RT_\xi}$$

$$= 2k_{ij}^{\circ} \times N_T \times C_{ij} \times \left(\frac{T_g}{T_\xi - T_g}\right) \exp(-E_{ij}/RT_\xi) \qquad (13)$$

Equation (13) is essentially of the Arrhenius type, in which the gas temperature T_g has, however, been substituted by the characteristic temperature T_ξ which defines the distribution function of vibro-rotationally excited molecules ij^* in their ground electronic state. To a first approximation one can take for k_{ij}° the appropriate crude collision values (see, however, below). With the assumption that T_ξ is the same for all molecular species in their ground electronic state, all the k_{ij}^{D} of interest can be calculated once T_ξ is known. T_ξ can easily be calculated by inserting in equation (13) the values of k_{ij}° and E_{ij} appropriate for H_2 and by equating this expression to the value of $k_{H_2}^{D}$ determined from the experiments and using the associated value of T_g.

$k_{N_2}^{D}$ can then be evaluated for all the conditions investigated and compared with values derived from the experiments.

In *Figure 17* values of T_g and T_ξ calculated at different pressures have been plotted as a function of $\langle W_{H_2O} \rangle$ for $R = 1$ and at 19 torr for $R = 3$. The trend from cold plasma conditions to the equilibrium conditions of thermal plasmas is apparent from this figure which shows that when the pressure is

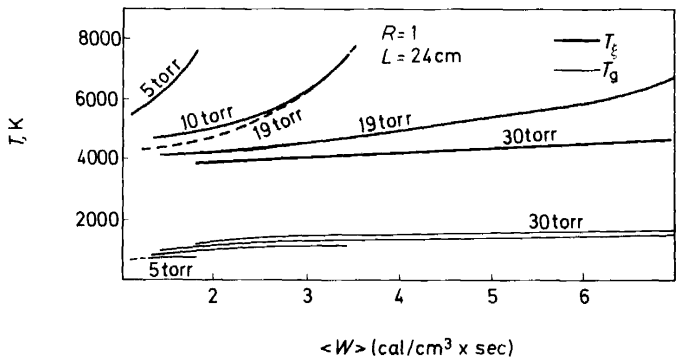

Figure 17. Vibro-rotational temperatures T_ξ and gas temperatures T_g calculated at different pressures as a function of power density $\langle W \rangle$ (broken line $R = 3$) (Ref. 14b).

increased from 5 to 30 torr T_g increases while T_ξ decreases, indicating that the two temperatures will merge when 'thermal' conditions are approached.

Calculated concentrations of hydrogen atoms at various pressures have been plotted in *Figure 18*, together with the corresponding degree of dissociation x_{H_2} for $R = 1$ and at 19 torr for $R = 3$. The same quantities have been

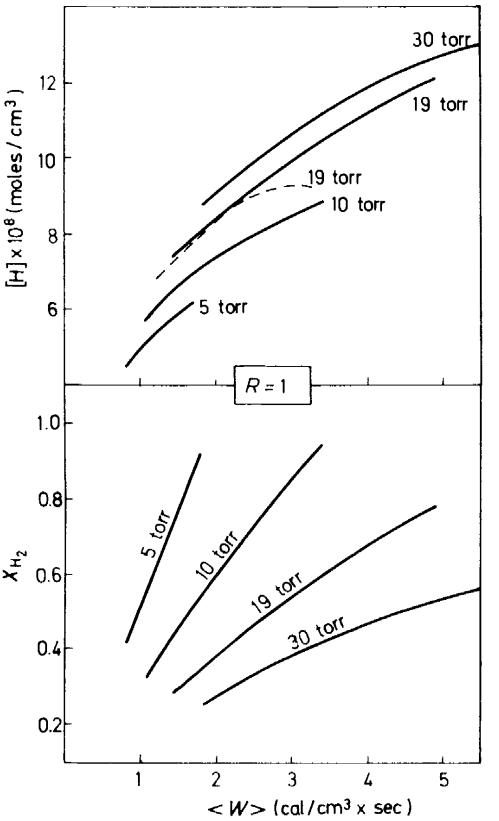

Figure 18. Plots of the concentrations of H atoms and of the corresponding degree of hydrogen dissociation (X_{H_2}) as a function of power density at different pressures (Ref. 14b).

reported in *Figure 19* for nitrogen. The latter concentrations have been calculated by applying equation (8) to N_2 dissociation after appropriate selection of the various constants.

In *Figure 20* calculated values of $k^D_{N_2}[N_2]^\circ$ have been plotted as a function of $\langle W_{H_2O} \rangle$ together with the experimental values derived as specified above.

If values of $k^D_{N_2}[N_2]^\circ_{exp}$ and $k^D_{N_2}[N_2]^\circ_{calc}$ in *Figure 20* are compared *vertically*, i.e. at the same value of $\langle W_{H_2O} \rangle = W_{H_2O}/\pi r_T^2 L = \langle W \rangle_{r_T}$, the disagreement can indeed be quite large depending on conditions. It is, however, possible to fit the experimental data to the calculated ones, *horizontally*, by successive approximations of T_g. The meaning of this fitting is that the experimental data should actually be plotted as a function of an "effective" $\langle W \rangle_{r_{eff}}$ given by $W_{H_2O}/\pi r_{eff}^2 L$. Values of r_{eff} calculated from this fitting procedure

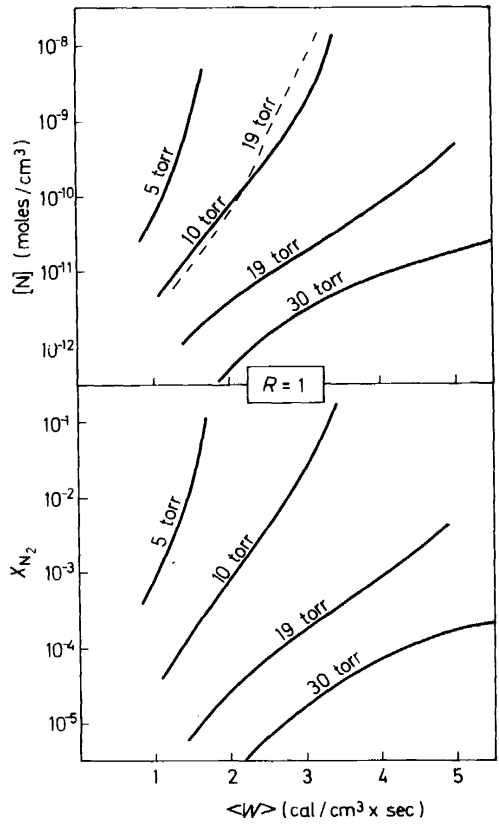

Figure 19. Plots of the concentrations of N atoms and of the corresponding degree of nitrogen dissociation (X_{N_2}) as a function of power density at different pressures (Ref. 14b).

have been plotted in *Figure 21* as a function of $\langle W \rangle_{r_T}$ for various conditions, together with the observed radii r_p of the more intensely luminous region of the plasma, as obtained from photographic evaluation.

It can be appreciated that r_{eff} parallels r_p under all conditions and $r_p < r_{eff} < r_T$; $r_{eff} - r_p$ is somewhat dependent on pressure, being larger at 5 torr. At this pressure the boundaries of the luminous region are not sharply defined and the central column of the plasma degrades into a blurred region.

The meaning of this type of fitting resides in the differences between the model of a uniform plasma utilized in the calculations and the actual discharges which all show a more or less contracted column. A rigorous treatment of the contracted plasma column would be of great complexity but the empirical correction of the radius which substitutes r_{eff} for r_T suggests that the total power W_{H_2O} delivered by the field to the gas is actually concentrated in a volume smaller than the geometrical one and related to the more intensely luminous volume of the plasma column. While on the whole the proposed model leads to reasonable results, it seems appropriate to comment further on the meaning of T_ξ which characterizes the Boltzmann distribution of

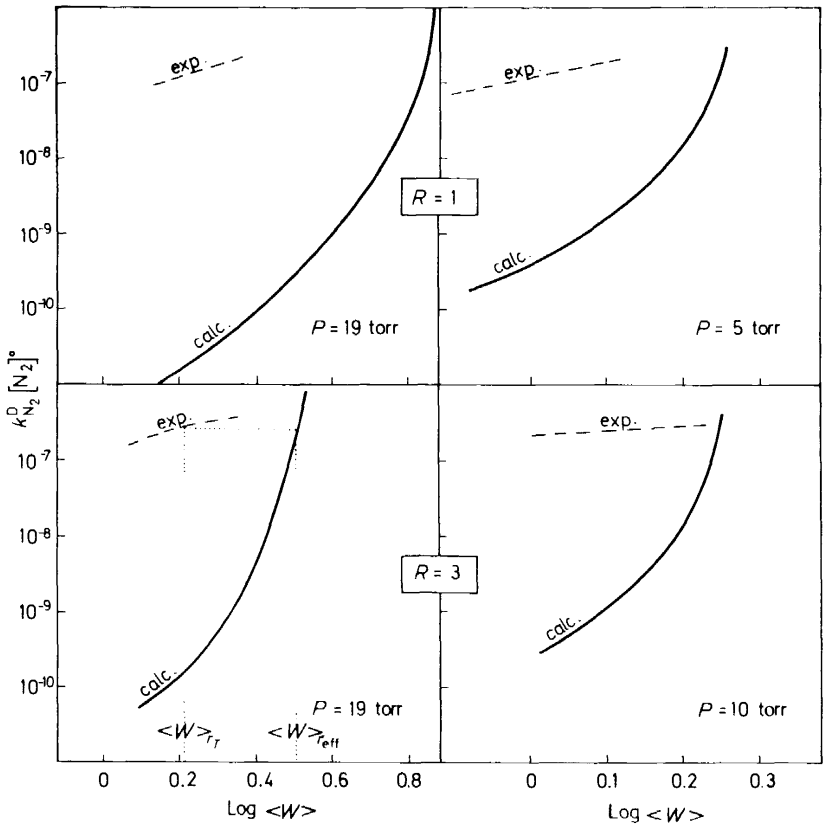

Figure 20. Experimental and calculated rates of nitrogen dissociation as a function of the power density $\langle W \rangle$ for different conditions. Dotted lines in the lower left quarter illustrate the fitting procedure (Ref. 14b).

vibro-rotationally excited molecules and plays in this model the role played by the gas temperature in purely thermal reactions.

The internal energy (vibrational + rotational) of a gas characterized by a sufficiently high vibro-rotational temperature T_ξ is $\simeq 2RT_\xi$ (cal/mole). For sufficiently high T_V and T_R one can therefore write

$$T_\xi \simeq \tfrac{1}{2}(T_V + T_R) \tag{14}$$

A comparison between the values of T_ξ derived from the experiments and the spectroscopic values of T_V and T_R of Ref. 11 shows that T_ξ is more than twice the value expected from (14).

The observed discrepancy should be traced back to the approximation made in assigning a crude collision theory value to k°_{ij}, independent of the energy level ξ considered (equation (12)).

Even on the basis of a purely collisional model a change of k°_{ij} with ξ is expected. In fact the bond length of H_2 in its ground *vibrational* state ($v = 0$) is 0·74 Å, whereas in the topmost vibrational level ($v = 14$) the bond length

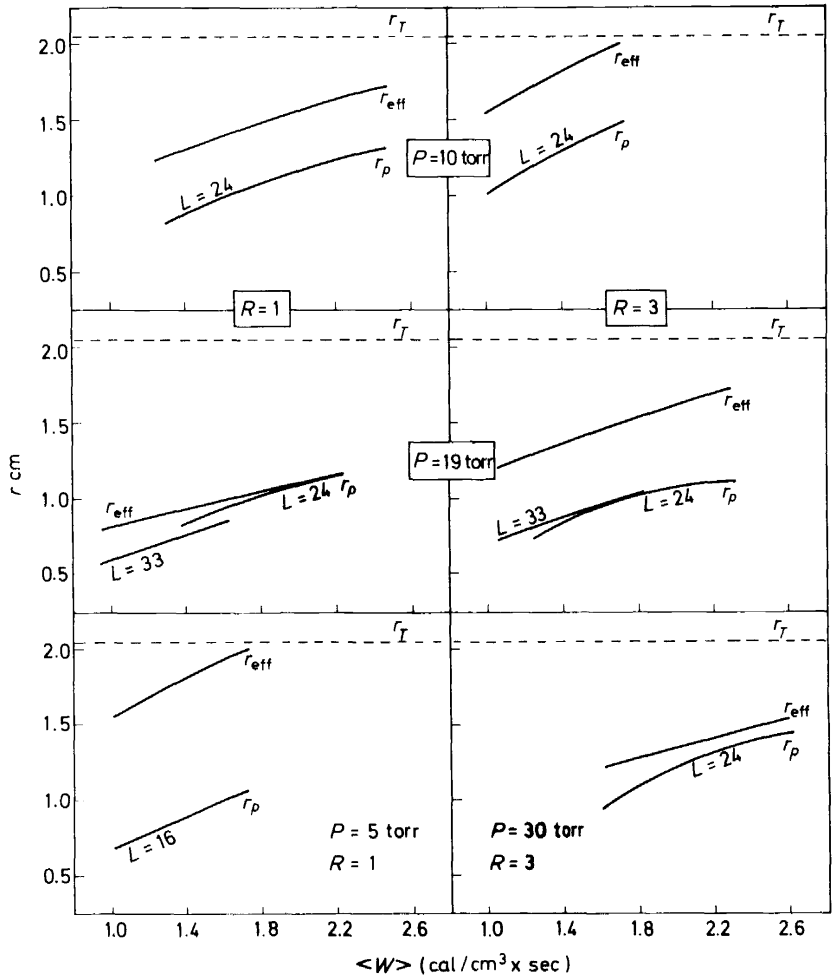

Figure 21. A comparison of the 'effective" plasma radius (r_{eff}) with the geometrical tube radius (r_T) and with the radius of the luminous region of the plasma (r_p) for different conditions and variable power density $\langle W \rangle$ (Ref. 14b).

is about 3.5 Å. This would cause a 20-fold increase between k°_{ij} ($v = 0$) and k°_{ij} ($v = 14$).

The problem of the *a priori* calculation of rates of thermal dissociation of diatomic molecules is, however, much more complex, and reference should be made to the work of Pritchard *et al.*[5] (see also refs 6, 7). According to Pritchard's treatment the rate of dissociation is related to the translational–vibrational transition probability, an increasing function of v, as well as to the probabilities of vibration–vibration transitions.

In the light of Pritchard's work it appears that k°_{jj} in equation (12) should actually be expressed as an increasing function of ξ. A convenient form is

$$k^\circ_{ij}(\xi)/k^\circ_{ij}(0) = e^{B\xi} \tag{15}$$

Equation (12) then becomes

$$k_{ij}(\xi) = 2k_{ij}^{\circ}(0)\, e^{B\xi} \times \exp\left[-(E_{ij} - \xi)/RT_g\right] \tag{16}$$

and equation (13) is transformed into

$$k_{ij}^{D} = 2k_{ij}^{\circ}(0) \exp(BE_{ij}) \times \exp(-E_{ij}/RT_{\xi})\,(T_g/\{T_{\xi} - T_g + RBT_{\xi}T_g\}) \times N_T \tag{17}$$

If (17) instead of (13) is utilized to calculate T_{ξ}, the new values of T_{ξ} will be smaller the higher the value of B, e.g. with $k_{H_2}^{\circ}(E_{H_2})/k_{H_2}^{\circ}(0) = 1.4 \times 10^2$ or 7×10^2, T_{ξ} will be lowered from 7000 K to 4000 K or 3500 K respectively ($T_g \simeq 1400$ K). The ratio $k_{H_2}^{D}/k_{N_2}^{D}$, which is $1{\cdot}8 \times 10^{-4}$ when $T_{\xi} = 7 \times 10^3$ K, would become 8.4×10^{-5} if $T_{\xi} = 4 \times 10^3$ K and $B_{H_2} = B_{N_2}$. It is, however, sufficient that $B_{N_2} = 1.2\, B_{H_2}$ for this ratio to become one order of magnitude larger.

The above considerations show that one cannot attach too much significance to *absolute* values of T_{ξ} unless values of B_{ij} can be determined. The reported trends of T_{ξ} and the fitting procedure do, however, maintain their validity.

THE CONVERSION OF METHANE INTO ACETYLENE

It has already been pointed out that this reaction proceeds at a much faster rate than the synthesis of HCN under similar discharge conditions. According to the discussion presented above the slow step of the synthesis is N_2 dissociation, a comparatively slow process even under discharge conditions. Data derived mostly from shock-tube experiments indicate that unimolecular decomposition of CH_4 is regulated by the rates of either step (a) or (b) below:

$$CH_4 \begin{cases} \xrightarrow{(a)} CH_3 + H \\ \xrightarrow{(b)} CH_2 + H_2 \end{cases}$$

The study of the conversion of CH_4 into C_2H_2 under discharge conditions of moderate pressure does therefore provide the opportunity of applying the dissociation mechanism discussed above to either step (a) or (b), assumed to be rate determining for the conversion, and to check the fitness of this model for a rationalization of the kinetic data. Acetylene represents the main product of the reaction. Traces of ethane have been detected at high flowrates while polymer deposition is of the order of five per cent at 20 torr.

Values of the percentage of CH_4 converted into $C_2H_2(\beta)$ obtained with sampling probes positioned at three different axial distances have been plotted in *Figure 22* as a function of the distance from the upper electrode for different flowrates and for three values of the power density.

Figure 23 shows the values of β, determined below the reaction zone, plotted as a function of the total power density for methane flowrates (Φ_{CH_4}) from 2 to 21.5 l. (s.t.p.)/min.

The effect of pressure on the conversion is illustrated in *Figure 24*. Values of β as a function of power density for three different CH_4/H_2 ratios at a constant methane flowrate of 10 l. (s.t.p.)/min are reported in *Figure 25*.

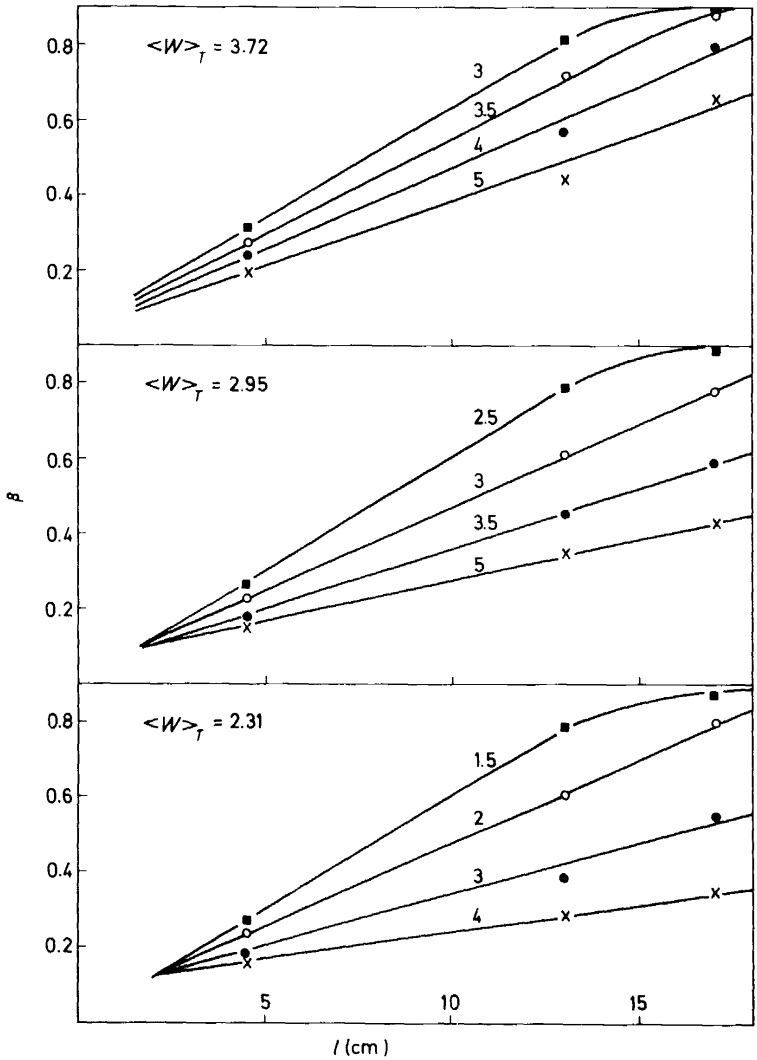

Figure 22. Plots of the percentage conversion of methane into acetylene (β) as a function of the axial distance l for different power densities $\langle W_T \rangle$ (cal cm^{-3} sec^{-1}) and flowrates of methane (l.(s.t.p.)/min) (Ref. 15).

The discussion of these data will be based on the assumption that path (a) above is rate determining.

According to the mechanism proposed for molecular dissociation under discharge conditions step (a) should proceed via bimolecular thermal dissociation from vibro-rotationally excited levels of CH_4. The vibro-rotational temperature T_r is assumed to be the same for both CH_4 and H_2. The rate of dissociation of H_2 in the discharge (mole cm^{-3} sec^{-1}) is given by

$$- \mathrm{d}[H_2]/\mathrm{d}t = k_{H_2} K_{H_2} N [H_2] \qquad (18)$$

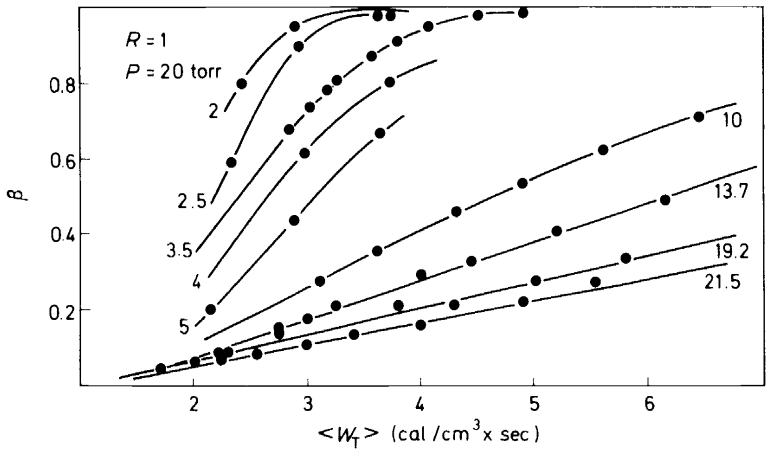

Figure 23. Plots of the percentage conversion of methane into acetylene (β) as a function of power density $\langle W_T \rangle$ for different flowrates of methane (l.(s.t.p.)/min) (Ref. 15).

with $N = P/RT$(mole cm^{-3})

$$k_{H_2} = k^{\circ}_{H_2} \times \exp(B_{H_2} 104 \times 10^3)$$

where $k^{\circ}_{H_2}$ (cm^3 mole^{-1} sec^{-1}) is the Arrhenius pre-exponential factor according to crude collision theory, and B_{H_2} is the constant which accounts for the dependence of the pre-exponential factor on the vibro-rotational energy ξ. 104×10^3 (cal/mole) is the dissociation energy of H_2,

$$K_{H_2} = \exp(-104 \times 10^3/RT_\xi)\left(\frac{T_g}{T_\xi - T_g + RB_{H_2}T_\xi T_g}\right) \qquad (19)$$

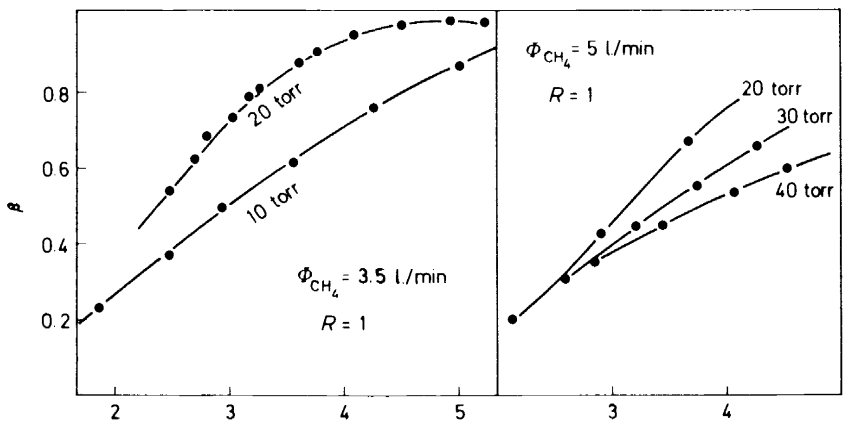

Figure 24. β as a function of $\langle W_T \rangle$ at different pressures (Ref. 15).

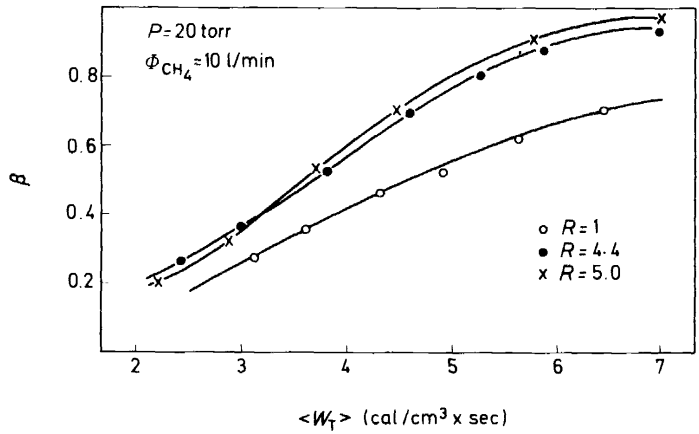

Figure 25. β as a function of $\langle W_T \rangle$ for different $[CH_4]/[H_2]$ ratios R (Ref. 15).

The rate expression for $CH_4 \xrightarrow{(a)} CH_3 + H$ will be

$$- d[CH_4]/dt = k_{CH_4} K_{CH_4} N [CH_4] \tag{20}$$

with

$$k_{CH_4} = k^{\circ}_{CH_4} \exp(B_{CH_4} 104 \times 10^3)$$

and

$$K_{CH_4} = \exp(-104 \times 10^3 / R T_\xi) \left(\frac{T_g}{T_\xi - T_g + R B_{CH_4} T_\xi T_g} \right) \tag{21}$$

104×10^3 (cal/mole) is in this case[19] the activation energy for path (a). The following energy balance can be written

$$\langle W \rangle_T = k_{H_2} \bar{K}_{H_2} N \Delta H_{H_2} [\bar{H}_2] + k_{CH_4} \bar{K}_{CH_4} N \Delta H_{CH_4} [\bar{CH}_4] \tag{22}$$

with W_T total power delivered to the plasma. ($\Delta H_{H_2} = 104 \times 3^3$ cal/mole; $\Delta H_{CH_4} = 45 \times 10^3$ cal/mole). In this expression $[\bar{H}_2]$, $[\bar{CH}_4]$, $\bar{K}_{H_2}$, $\bar{K}_{CH_4}$ are the values of $[H_2]$, $[CH_4]$, K_{H_2} and K_{CH_4} averaged along the reactor's axis. The power utilized for the *endothermic* conversion is, within one per cent,

$$W_T - W_{H_2O} = \hat{\Phi}_{CH_4} \beta_L \Delta H_{CH_4} \tag{23}$$

W_{H_2O} is the power collected by the water jacket and $\hat{\Phi}_{CH_4}$ (mole sec^{-1}) is the molar flowrate of CH_4. One can therefore identify $\langle W_T - W_{H_2O} \rangle$ with $\langle W \rangle_{CH_4}$ and $\langle W \rangle_{H_2O}$ with $\langle W \rangle_{H_2}$. Under the assumption that T_ξ is the same for both H_2 and CH_4, and putting $B = (B_{H_2} + B_{CH_4})/2$, one can write

$$\bar{K}_{H_2} = \bar{K}_{CH_4} = \bar{K} = \exp(-104 \times 10^3 / R T_\xi) \left(\frac{T_g}{T_\xi - T_g + R B T_\xi T_g} \right)$$

The energy balance (22) can then be split into two terms:

$$\langle W\rangle_{H_2} = k_{H_2} \times \bar{K} \times N \times (\bar{H}_2)\,\Delta H_{H_2} \tag{24}$$

$$\langle W\rangle_{CH_4} = k_{CH_4} \times \bar{K} \times N \times (\bar{CH}_4)\,\Delta H_{CH_4} \tag{25}$$

The mass balance for the system consisting of the majority species H_2, H, CH_4 and C_2H_2 leads to the following expression for $[\bar{H}_2]$ and $[\bar{CH}_4]$

$$[\bar{H}_2] = \frac{(1-\bar{\alpha})(1+1.5\,R\bar{\beta})}{(1+R)+R\bar{\beta}+\bar{\alpha}(1+1.5R\bar{\beta})} \times P/RT_g \tag{26}$$

$$[\bar{CH}_4] = \frac{R(1-\bar{\beta})}{(1+R)+R\bar{\beta}+\bar{\alpha}(1+1.5R\bar{\beta})} P/RT_g \tag{27}$$

where $\bar{\alpha}$ is the degree of dissociation of hydrogen averaged along the reactor's axis and $R = [CH_4]^\circ/[H_2]^\circ$. From the plots of *Figure 22* one appreciates that a value $\bar{\beta} = \beta_{L/2} \doteq \frac{1}{2}\beta_L$ is correct up to about $\beta = 0.9$. Equations (24) and (25) provide a system of two equations in the two unknowns $\bar{\alpha}$ and $\bar{K}$ which can therefore be determined from the experimental data. One has:

$$\begin{cases} (1-\bar{\alpha}) = \dfrac{\langle W\rangle_{H_2}}{\langle W\rangle_{CH_4}} \times \dfrac{k_{CH_4}}{k_{H_2}} \times \dfrac{\Delta H_{CH_4}}{\Delta H_{H_2}} \times \dfrac{R(1-\bar{\beta})}{(1+1.5\,R\bar{\beta})} & (28') \\ N\bar{K} = \dfrac{\langle W\rangle_{H_2}}{k_{H_2}\Delta H_{H_2}} \times \dfrac{(1+R)+R\bar{\beta}+\bar{\alpha}(1+1.5\,R\bar{\beta})}{(1-\bar{\alpha})(1+1.5\,R\bar{\beta})} \times \dfrac{RT_g}{P} & (28'') \end{cases}$$

The ratio k_{CH_4}/k_{H_2} is unfortunately unknown because of our ignorance of the values of B_{H_2} and of B_{CH_4}. We shall therefore arbitrarily select the maximum value for this ratio which allows values $0 < \alpha < 1$ to be obtained from the solution of system (28) for *all* the experimental points. This value is $k_{CH_4}/k_{H_2} = 0.2$. Simple transformation of equations (28'), (28'') gives

$$N\left(\frac{NKk_{CH_4}}{\langle W\rangle_T}\right) = \frac{(1+R)+R\beta+\bar{\alpha}(1+1.5\,\bar{\beta}R)}{45\times10^3\times11.6\,(1-\bar{\alpha})(1+1.5\,\bar{\beta}R)+R(1-\bar{\beta})} \tag{28'''}$$

In *Figure 26* $\log N(NKk_{CH_4}/\langle W\rangle_T)$ determined at different pressures and different R has been plotted as a function of $\log 1/(1-\bar{\alpha})$. The full line for $R = 1$ collects *all* the points determined at 10, 16, 20, 30 and 40 torr within the scattering indicated by the vertical bars. The broken lines refer to the data for $R = 4.4$ and 50.

Values of NKk_{CH_4} have been calculated from the plots of *Figure 22* and equations (28'), (28'') and plotted as a function of the axial distance l in *Figure 27*, where they are compared with values of the first order rate constants derived according to a plug flow model of the reactor (k_p) or to an approximately laminar flow model (k_l). Values of NKk_{CH_4} derived from these plots have been included in *Figure 26* (×). The corresponding dependence of α on l is illustrated in *Figure 28*.

The black circles are values of α calculated from the expression:

$$\frac{2[H]}{2N-[H]}\frac{\Phi}{\pi r_T^2 l} = \frac{2\langle W_{H_2}\rangle}{\Delta H_{H_2}} - \{k'[H]+k''(N-[H])[H]^2+k'''[H]^3\} \tag{29}$$

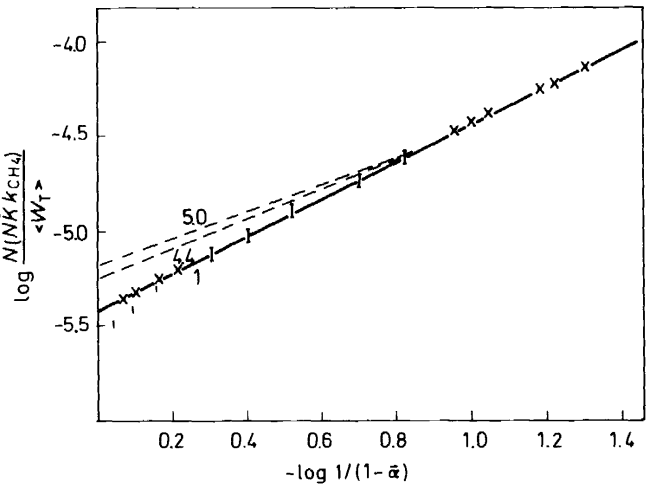

Figure 26. Plots of $\log N\left(\frac{N\bar{K}k_{CH_4}}{\langle W_T \rangle}\right)$ as a function of $\log 1/(1-\bar{\alpha})$. Full line $R = 1$ all pressures. Dashed lines $R = 4.4$, and 50. α is the extent of hydrogen dissociation (Ref. 15).

which represents the kinetics of H atom generation in an approximately laminar reactor. A two temperatures model has been utilized in this calculation with the temperature of the central luminous region of the plasma higher than the dark periphery.

The energy yield of the process defined as $\eta = \langle W \rangle_{CH_4}/\langle W \rangle_T$ can easily be derived from equations (28′), (28″)

$$\eta = \left(1 + \frac{k_{H_2}}{k_{CH_4}} \times \frac{\Delta H_{H_2}}{\Delta H_{CH_4}} \times \frac{(1-\bar{\alpha})(1+1.5R\bar{\beta})}{R(1-\beta)}\right)^{-1} \tag{30}$$

In *Figure 29* η has been plotted as a function of $\bar{\beta}$ for different values of $\bar{\alpha}$ and for $R = 1$ and $R = 50$.

This figure is instructive. It shows the increase of η with increasing $\bar{\alpha}$ and with increasing R but it also shows that an increase of $\bar{\beta}$, at given $\bar{\alpha}$ and R, causes η to decrease, a rather unexpected result. The reason for this behaviour resides in the detrimental influence of the hydrogen which obviously increases when the conversion of methane into C_2H_2 and H_2 increases.

Values of η predicted by (30) are in full agreement with the experimental observations.

From plots of β as a function of $1/\Phi_{CH_4}$ at constant $\bar{\alpha}$ one can extrapolate at very large Φs and obtain the minimum β compatible with the given $\bar{\alpha}$. The maximum value of η to be expected for large R, large Φ, $\bar{\alpha} = 0{\cdot}85$ and correspondingly high values of $\langle W \rangle_T$ is 0.45 ± 0.05. This value should be compared with the maximum yield obtained in the synthesis of HCN, namely 0.006. The maximum measured value of η is 0.30. The results presented above show that the energy balance equations (28′), (28″) based on the proposed mechanism of molecular dissociation do in fact allow simple rationalization of the kinetic data.

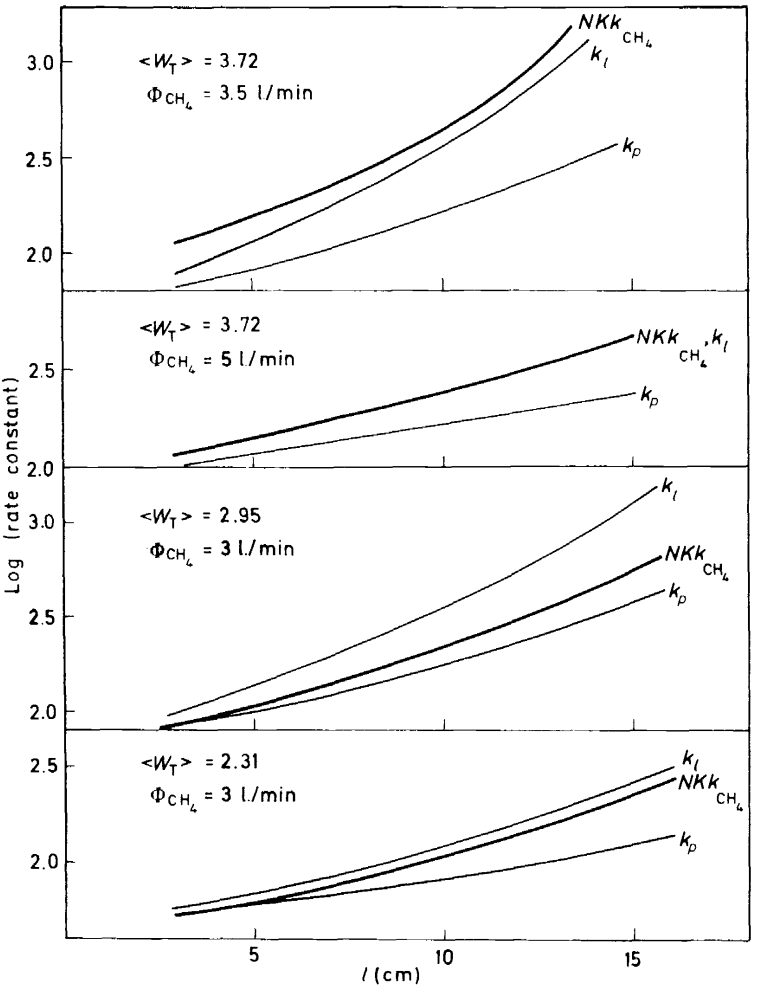

Figure 27. Plots of the rate constants $N\bar{K}\,k_{CH_4}$, k_l and k_p as a function of axial distance l for different conditions (Ref. 15).

These results indicate that the 'clue' to the understanding of the kinetics of CH_4 decomposition in the discharge is represented by the relationship between K and α brought out by the kinetic analysis of the data. The expression for K is

$$K = \exp\left(-\frac{104 \times 10^3}{RT_\xi}\right)\left(\frac{T_g}{T_\xi - T_g + RBT_\xi T_g}\right)$$

and the observed dependence on α should therefore be attributed to an increase of T_ξ with α, i.e. the vibro-rotational temperature of the molecular species in their ground electronic state increases with increasing dissociation of the hydrogen. An increase of T_ξ means an increased population of higher vibro-rotational levels. A change of T_ξ can be brought about essentially by two

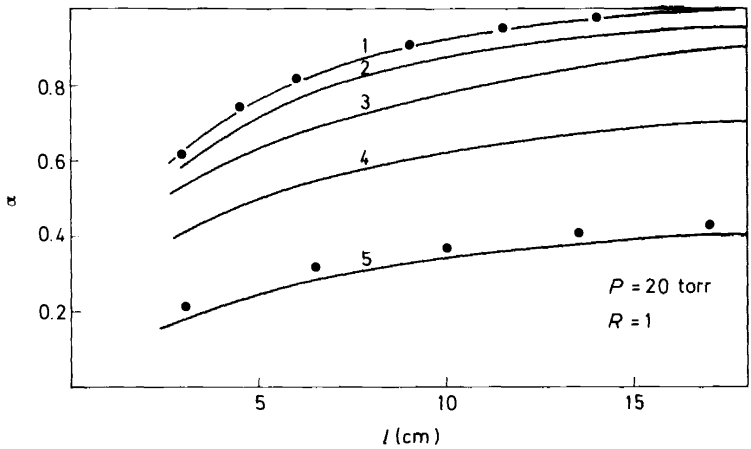

Figure 28. Plots of the extent of hydrogen dissociation α as a function of axial distance l (black circles calculated) (Ref. 15).

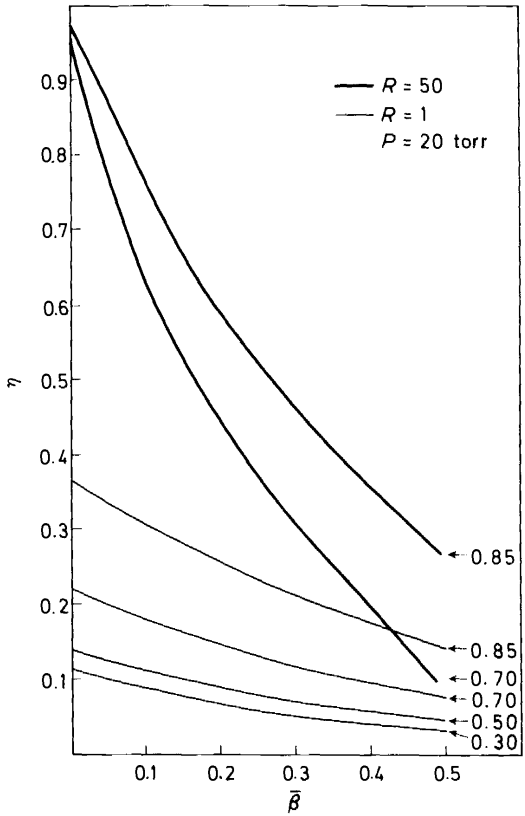

Figure 29. Energy yield of the conversion of methane into acetylene as a function of $\bar{\beta}$ and $\bar{\alpha}$ for two $[CH_4]/[H_2]$ ratios (calculated) (Ref. 15).

factors. (i) An increase of the electron temperature T_e, a function of the reduced field strength X/P and of the composition. Higher T_e would in fact cause a rapid increase of the rates of excitation of the higher vibro-rotational levels from the lower ones and this would increase T_ξ, other things being equal. If for simplicity we consider pure molecular hydrogen the value of T_e is uniquely determined by X/P. However, at the same value of X/P *atomic* hydrogen would have a very different T_e. The closest species to atomic hydrogen for which data can be found in the literature is He and these data show that for $X/P = 1$ (volt cm^{-1} $torr^{-1}$) $T_e(He) \simeq 12\,000$ K and $T_e(H_2) = 3\,000$ K[10]. An increase of T_ξ can therefore be expected as molecular hydrogen is progressively converted into atomic hydrogen. (ii) The value of T_ξ, other things being equal, is also determined by the probability of collisional deactivation of the vibro-rotationally excited levels, an increasing function of the energy of these levels and of the gas temperature[5]. The nature of the deactivating particle is obviously important and a change from an essentially molecular to an essentially atomic gas is likely to lead to an increase of the probability of deactivation, hence a decrease of T_ξ. These are in our opinion the main factors that might contribute to the observed dependence of K on α.

The energy balance equation imposed on our system requires that K should vary with gas composition at constant $\langle W \rangle_T$. The fact that this energy balance allows one to rationalize a large amount of kinetic data is certainly a point in its favour, but this implies that the system must adjust itself to the modified composition by a compensating increase of its vibro-rotational temperature T_ξ. This is an argument which definitely deserves further investigation.

THE PRODUCTION OF HYDROGEN ATOMS

At this stage the obvious idea would be to verify the model on a 'simpler' reaction like the dissociation of H_2 by measuring the effectiveness of these discharges in producing hydrogen atoms under variable conditions of power, pressure, flowrate and gas purity. The main difficulty in this pressure range and at the power levels which can be utilized resides in the experimental determination of the concentration of the hydrogen atoms. This difficulty has, however, been circumvented by a method which, although not very accurate, allows reasonable estimates to be made.

The reactor of *Figure 8* has been modified by subdividing the water jacket into a number of sectors in series, separated by O-rings, and by adding a metal heat exchanger at the lower end of the reactor. By measuring at the outlet of each sector the temperature of the water flowing at a constant and metered rate it is possible to derive the power transferred from the plasma to the cooling water in each sector of the system. The total power collected by the water is $W_T = f V_p I_p/2$ with $f = 0.95 \pm 0.03$. V_p and I_p are the d.c. voltage and intensity respectively and the value of f indicates good coupling between the circuit and the plasma. The results of these measurements are illustrated in *Figure 30*. The lower curve in this figure was obtained at a flow rate of the hydrogen of 0.08 s.t.p. litres/min. When the flowrate is progressively increased the W_{H_2O}/l curves are modified as shown in the figure, and *Figure 31* shows the effect of changes of the power input to the plasma at a constant

flowrate. The meaning of the curves of *Figures 30* and *31* is rather straightforward. If W_T is the total power collected by the water and W_L the power collected by the water within the electrodes placed at a distance L or, more

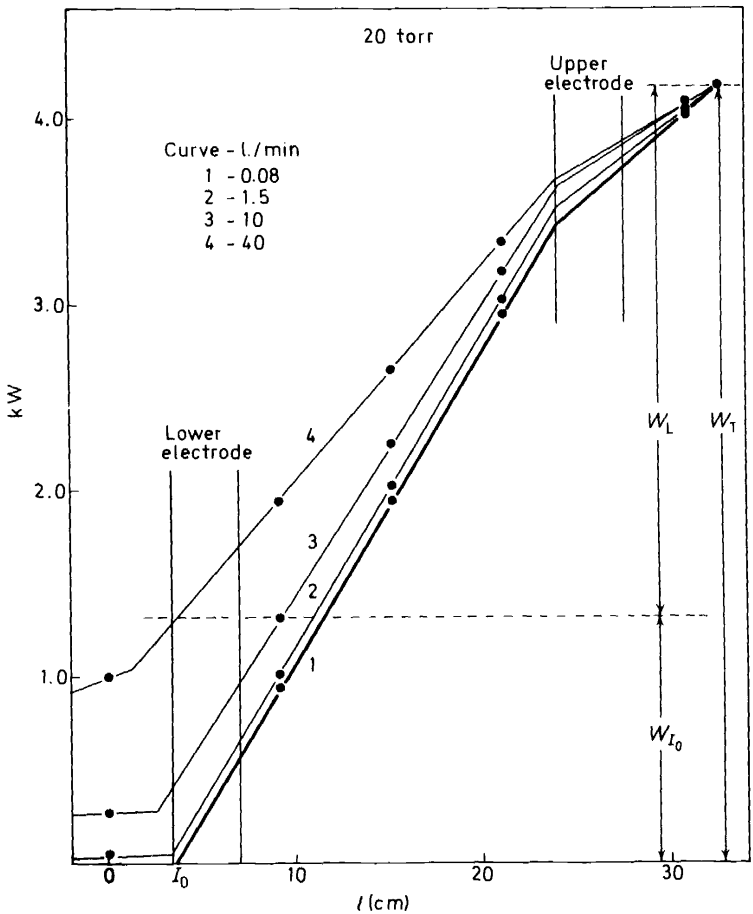

Figure 30. Plots of the power collected by the water jacket as a function of the axial distance for a fixed W_T and variable flowrates of hydrogen (l./min). Circles mark the positions of the O-rings (Ref. 16).

generally, within the actual length of the applied r.f. field, one has: $W_T - W_L = \hat{\Phi}\mathscr{H}$ where $\hat{\Phi}$ is the molar inlet flowrate of H_2 (mole/sec) and $\mathscr{H}$ the enthalpy of the discharged gas referred to one mole of inlet gas and given by

$$\mathscr{H} = \frac{2[H]}{2N - [H]} \times \tfrac{1}{2}\Delta H_{H_2} + \bar{C}_{p_{H_2}}(T_g - 298)\left(1 - \frac{[H]}{2N - [H]}\right) + \bar{C}_{p_H}(T_g - 298)\frac{2[H]}{2N - [H]} \qquad (31)$$

with $\alpha = [H]/(2N - [H])$. The value of the ordinate at $l = l_0$, where l_0 marks the beginning of the electric field, is therefore

$$W_{l_0} = W_T - W_L = \hat{\Phi}_{H_2} \alpha A(T_g) + D(T_g) \tag{32}$$

From this equation and equations (6), (7), (8), α and T_g can both be calculated with certain approximations. The results of these calculations are given in *Figure 32* where they are compared with values derived from equation (29) at radially uniform plasma temperatures T_g. Values of T_g range from 700 to 1300 K.

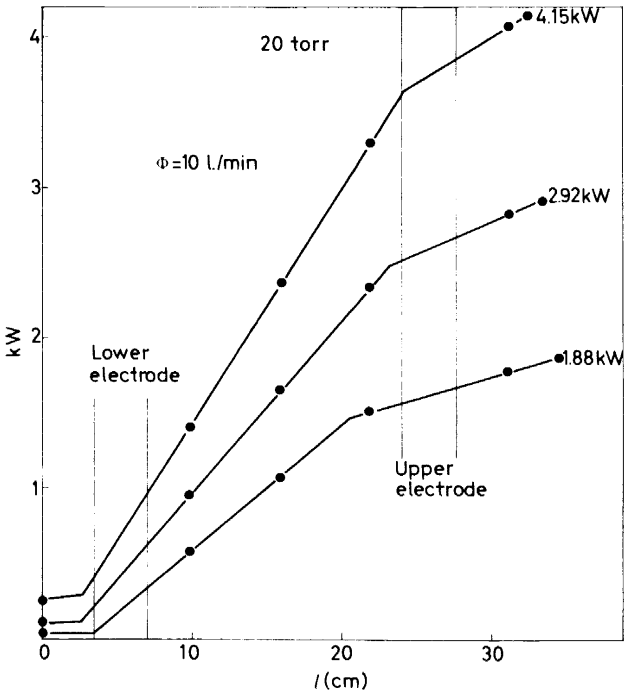

Figure 31. Plots of the power collected by the water jacket as a function of the axial distance for different $\langle W_T \rangle$ and a fixed hydrogen flowrate (Ref. 16).

It should be pointed out that values of α as derived from *Figures 30* and *31* represent radially averaged values of this quantity which should actually exhibit a pronounced radial profile as a consequence of the contraction of the plasma column (see refs. 14b, 15).

THE REDUCTION OF METAL OXIDES IN HYDROGEN

The reduction of CuO, NiO, PbO and ZnO injected axially into a cylindrical reactor of the type shown in *Figure 8* but with internal water cooled electrodes of copper, has been studied in a hydrogen plasma at pressures between 10 and 50 torr (r.f. = 8 MHz). The percentage of reduction β was

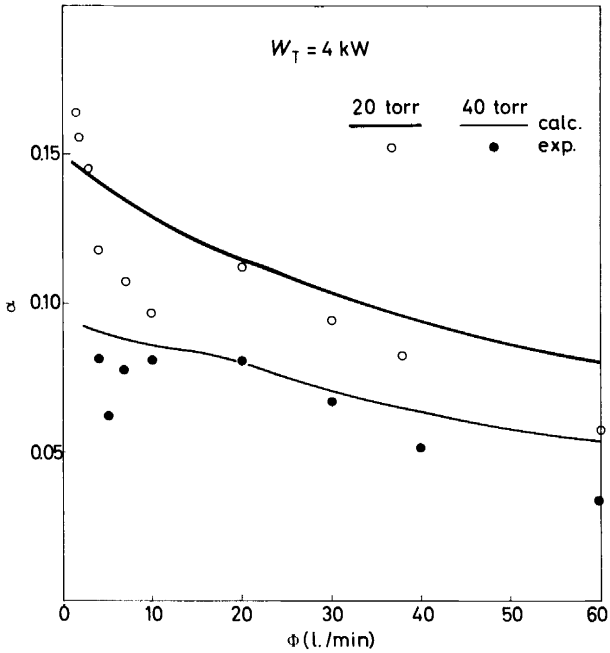

Figure 32. Observed and calculated values of the extent of hydrogen dissociation α as a function of hydrogen flowrate (Ref. 16).

determined from the differential reading of two calibrated flowmeters after condensation of the water. The specific rate of reduction k_s expressed in mole reduced per square centimetre of particle surface per second is related to β by the equation

$$\beta = k_s B \bar{\theta} 4\pi r_p^2 \tag{33}$$

where B is the number of particles per mole of the oxide, $\bar{\theta}$ the average residence time of the particle within the flame and r_p the radius of the supposedly spherical particle. Mass feed rates Φ_p of the powder ranged from 0.2 to 30 g/min. $\bar{\theta}$ was of the order of 10^{-2} sec.

While the reduction of ZnO and PbO leads to rapid evaporation of the low boiling metal, which then condenses on the reactor's wall, reduction of CuO and NiO is accompanied by the formation of an external layer of liquid (Cu) or solid (Ni) metal which progressively grows toward the interior. Evaporation is limited in the latter cases.

As shown in previous sections, concentrations of hydrogen atoms in this type of discharge are well above thermodynamic values corresponding to the gas temperature T_g. In the absence of the powder these concentrations can be calculated according to equation (8). In the presence of powder the first order term $k'[H]$ in this equation should be modified to account for the heterogeneous loss of atoms due to recombination and reaction at the particle's surface. An additional first order term must therefore be added, namely

$$\gamma' \tfrac{1}{4} \bar{c} [H] \times n_p \times 4\pi r_p^2 \tag{34}$$

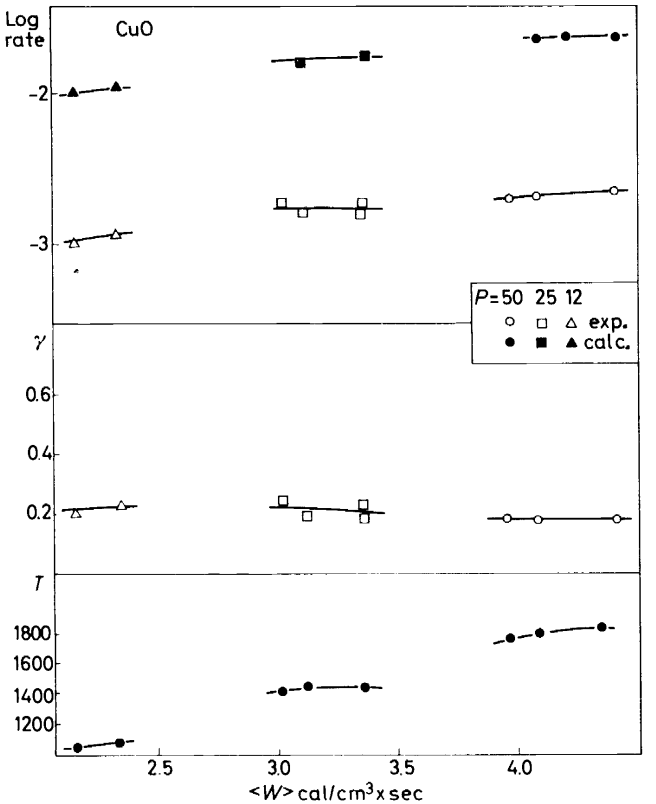

Figure 33. Semilogarithmic plots of $\frac{1}{4}\bar{c}$ [H], (filled symbols) and k_s (open symbols), and linear plots of γ and T_g as a function of $\langle W \rangle$ at various pressures for the reduction of copper oxide (CuO) (Ref. 17).

with $\bar{c}$ the mean square velocity of the H atoms at T_g, γ' the fraction of colliding atoms which is removed by recombination and reduction, and n_p the number of particles present per cm^3 of plasma. Calculation shows that for small values of Φ_p, hence of n_p, term (34) can actually be neglected in equation (8). A comparison is then possible between the experimental values of k_s (mole cm^{-2} sec^{-1}) and the rate of arrival of the H atoms at the particle surface $\frac{1}{4}\bar{c}$ [H] (atoms cm^{-2} sec^{-1}). This comparison is shown in *Figures 33* and *34* for CuO and ZnO respectively. Data for NiO and PbO are very similar. The ratio $2k_s/\bar{c}$ [H] will be called γ. *Figures 33* and *34* show the calculated values of γ, and include the gas temperatures T_g derived from the heat balance as previously discussed. When n_p is increased the contribution of term (34) becomes appreciable and the concentration of the hydrogen atoms therefore drops, with a corresponding decrease of k_s. Good correlation can be obtained between the observed decrease of β with increasing n_p and the corresponding decrease of [H] calculated as specified above with $\gamma' = \gamma$. The above results strongly suggest that the reaction responsible for reduction is $MeO + 2H = Me + H_2O$ with a negligible contribution from the reaction with molecular hydrogen.

The data reported in *Figures 33* and *34* indicate that the heterogeneous step in the reduction of these oxides by hydrogen atoms, at the particle temperatures of the experiments ($T_p > T_g$), is a comparatively fast process ($\gamma = 10^{-2}, 10^{-1}$) essentially not activated in the case of CuO and NiO (γ independent of T_g) and with an activation energy of the order of 3–6 kcal/mole for PbO and ZnO (γ is temperature dependent in these cases).

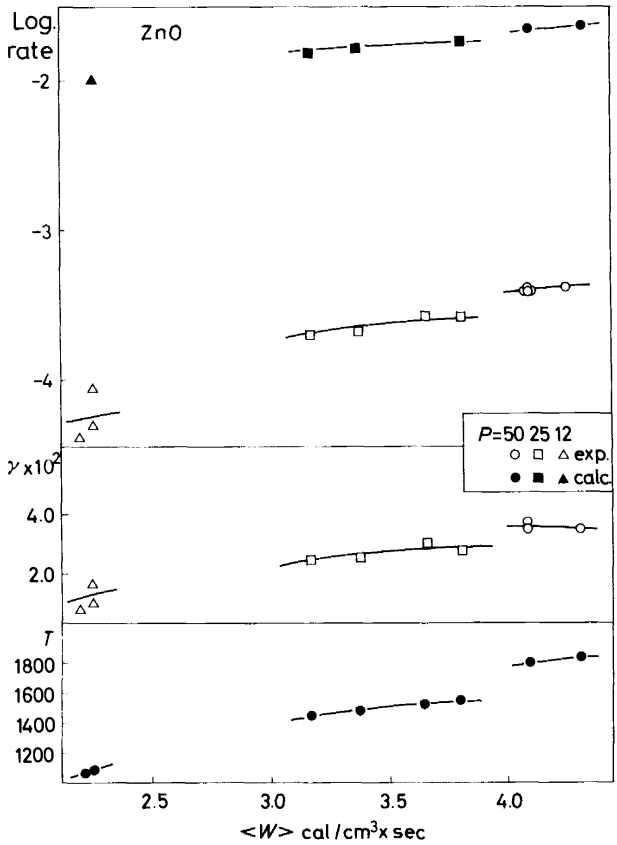

Figure 34. Semilogarithmic plots of $\frac{1}{4}\bar{c}$ [H] (filled symbols), and k_s (open symbols), and linear plots of γ and T_g as a function of $\langle W \rangle$ at various pressures for the reduction of zinc oxide (ZnO) (Ref. 17).

Alumina is not appreciably reduced in these plasmas because the reaction of Al_2O_3 with hydrogen atoms is still too slow at the particle temperature attainable in these systems. An appreciably higher activation energy is apparently present in this case. In *Figure 35* energy yields of the process in mole/joule are shown as a function of the molar feed rate of the oxide (mole/sec) for NiO and ZnO.

Experimental yields increase at first with increasing Φ_p, go through a maximum and then decrease.

This behaviour can be attributed to the observed change of the radial distribution of the powder within the plasma, which is rather uniform at small Φ_p but progressively concentrates into a narrow central channel with increasing Φ_p. Energy yields calculated on the assumption of a uniform radial distribution of the powder are given by the curves of *Figure 35*.

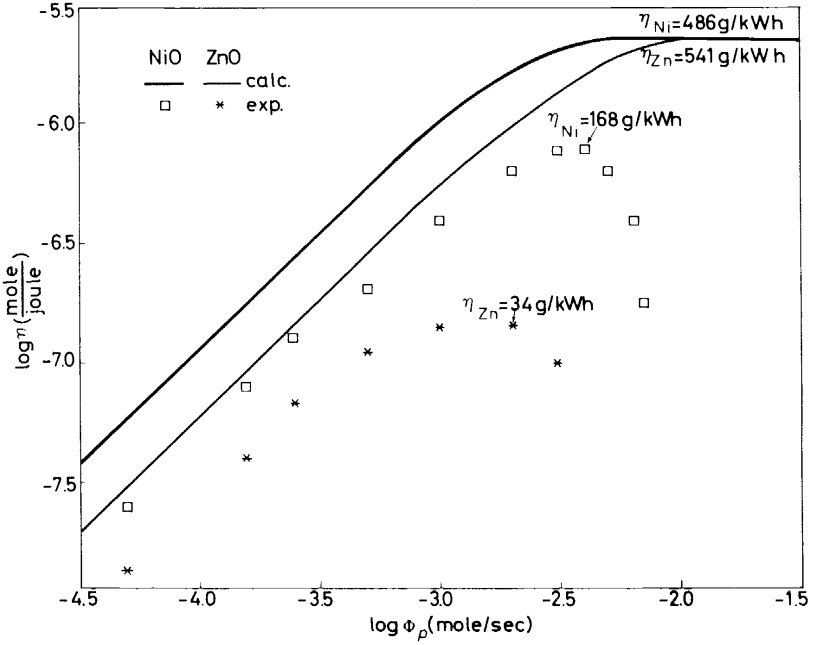

Figure 35. Energy yield for the reduction of nickel oxide and zinc oxide at 50 torr as a function of the molar feed rate Φ_p (Ref. 17).

Energy yields in the electrolytic processes for the preparation of zinc are between 250 and 300 g/kWh.

For a comparison of the present results with the behaviour of oxide particles injected into 'thermal' plasmas of argon and of argon + nitrogen one should refer to Ref. 20.

CONCLUSIONS

The use of r.f. gas discharges as chemical reactors in the pressure range 5–50 torr has brought out features which are characteristic of this intermediate range of pressures and make these discharges essentially different from both 'cold' and 'thermal' plasmas. The presence of a marked vibro-rotational disequilibrium appears to be responsible for the chemical 'activity' of these discharges and kinetic considerations based on this idea apparently allow a satisfactory rationalization of both homogeneous and heterogeneous processes. Interesting energy yields can be obtained in some of the processes examined. One point should be emphasized in this connection: in all systems

considered in this report the loss of hydrogen atoms by heterogeneous recombination at the reactor's wall or by homogeneous recombinations influences the observed energy yields.

In the synthesis of hydrogen cyanide yields are particularly low (less than one per cent of thermodynamic value) because the slow step of this reaction is nitrogen dissociation, a much slower process than the dissociation of hydrogen even under discharge conditions. The consequence is that *most* of the energy transferred by the r.f. field to the plasma is lost to the walls.

In the conversion of methane into acetylene competition for the field energy between hydrogen and methane is closer but hydrogen remains favoured, as clearly indicated by the results reported in *Figure 29*. In this case limiting yields at high flowrates can be predicted which attain 45 ± 5 per cent of a thermodynamic value of 250 g of acetylene per kWh. The limiting yields calculated for the reduction of metal oxides and reported in *Figure 35* correspond to $1/104 \times 10^3$ mole/calorie where 104×10^3 is the dissociation energy of molecular hydrogen. The meaning of this result is that for sufficiently high concentrations of the powders within the plasma *all* hydrogen atoms generated by the discharge are utilized for the heterogeneous process of reduction and are not therefore lost to the walls or in homogeneous recombinations.

Considerations such as those presented above can provide useful guidelines for the evaluation of possible applications of these plasmas.

REFERENCES

[1] *Kinetika i Termodinamica Khimicheski Reaktsii Nisko Temperaturnoi Plasme*, L. S. Polak (Ed.) Nauka: Moscow (1965).

[2] *The Applications of Plasmas to Chemical Processing*, R. F. Baddour and R. S. Timmins (Eds.) MIT Press: Cambridge, Mass. (1967).

[3] *Reactions under Plasma Conditions*. M. Venugopalan (Ed.) Wiley: New York (1971).

[4] (a) A. T. Bell, *Industr. Engng Chem. Fundam.* **11**, 209 (1972).
(b) in *Fundamentals of Plasma Chemistry*, A. T. Bell and J. Hollahan (Eds.) Wiley–Interscience: New York (1973).

[5] D. L. S. McElevain and H. O. Pritchard, *Thirteenth Symposium (International) on Combustion*, p 37. The Combustion Institute: Pittsburgh (1971). *J. Amer. Chem. Soc.* **92**, 5027 (1970).

[6] Ven H. Shui, J. P. Appleton and J. C. Keck, *Thirteenth Symposium (International) on Combustion*, p 21. The Combustion Institute: Pittsburgh (1971).

[7] L. S. Polak in *Reactions under Plasma Conditions*, M. Venugopalan (Ed.), Vol. 2, p 141. Wiley: New York (1971).

[8] B. B. Bronfin in *Chemical Reactions in Electrical Discharges*, p 423. Advances in Chemistry Series No. 80. American Chemical Society: Washington, DC (1969).

[9] H. Sabadil, *Beitr. Plasma Phys.* **53** (1971).

[10] H. S. W. Massey, *Electronic and Ionic Impact Phenomena*, Vol. 2, Clarendon Press: Oxford (1969).

[11] F. Cramarossa, G. Ferraro and E. Molinari, *J.Q.S.R.T.* **14**, 159 (1974).

[12] J. C. Polanyi, *Accounts Chem. Res.* **5**, 161 (1972).

[13] M. Burton and K. Funabashi in *Chemical Reactions in Electrical Discharges*, p 152. Advances in Chemistry Series No. 80, American Chemical Society: Washington, DC (1969).

[14] (a) P. Capezzuto, F. Cramarossa, G. Ferraro, P. Maione and E. Molinari; *Gass. Chim. Ital.* **103**, 1153 (1973).
(b) P. Capezzuto, F. Cramarossa, R. d'Agostino and E. Molinari, *Gazz. Chim. Ital.* **103**, 1169 (1973).

[15] P. Capezzuto, F. Cramarossa, P. Maione and E. Molinari, *Gazz. Chim. Ital.* **103**, 891 (1973). (English).

[16] Work in progress in this laboratory.

[17] P. Maione, P. Capezzuto, F. Cramarossa and E. Molinari, paper submitted for publication to *Gazz. Chim. Ital.* (English).
[18] S. Vepřek, *J. Chem. Phys.* **57**, 952 (1972).
[19] S. W. Benson and H. E. O'Neal, 'Kinetic data on gas phase unimolecular reactions *NSRDS-NBS 21* (1970), p 381.
[20] C. Borgianni, M. Capitelli, F. Cramarossa, L. Triolo and E. Molinari, *Combustion and Flame*, **13**, 181 (1969);
M. Capitelli, F. Cramarossa, L. Triolo and E. Molinari, *Combustion and Flame*, **15**, 23 (1970).